Supplementary Information - Conversion from coniferous to broadleaved trees can make European forests more climate-effective

Yao et al.

Contents

List of Figures

1 Supplementary Figures

Figure Legends/Captions

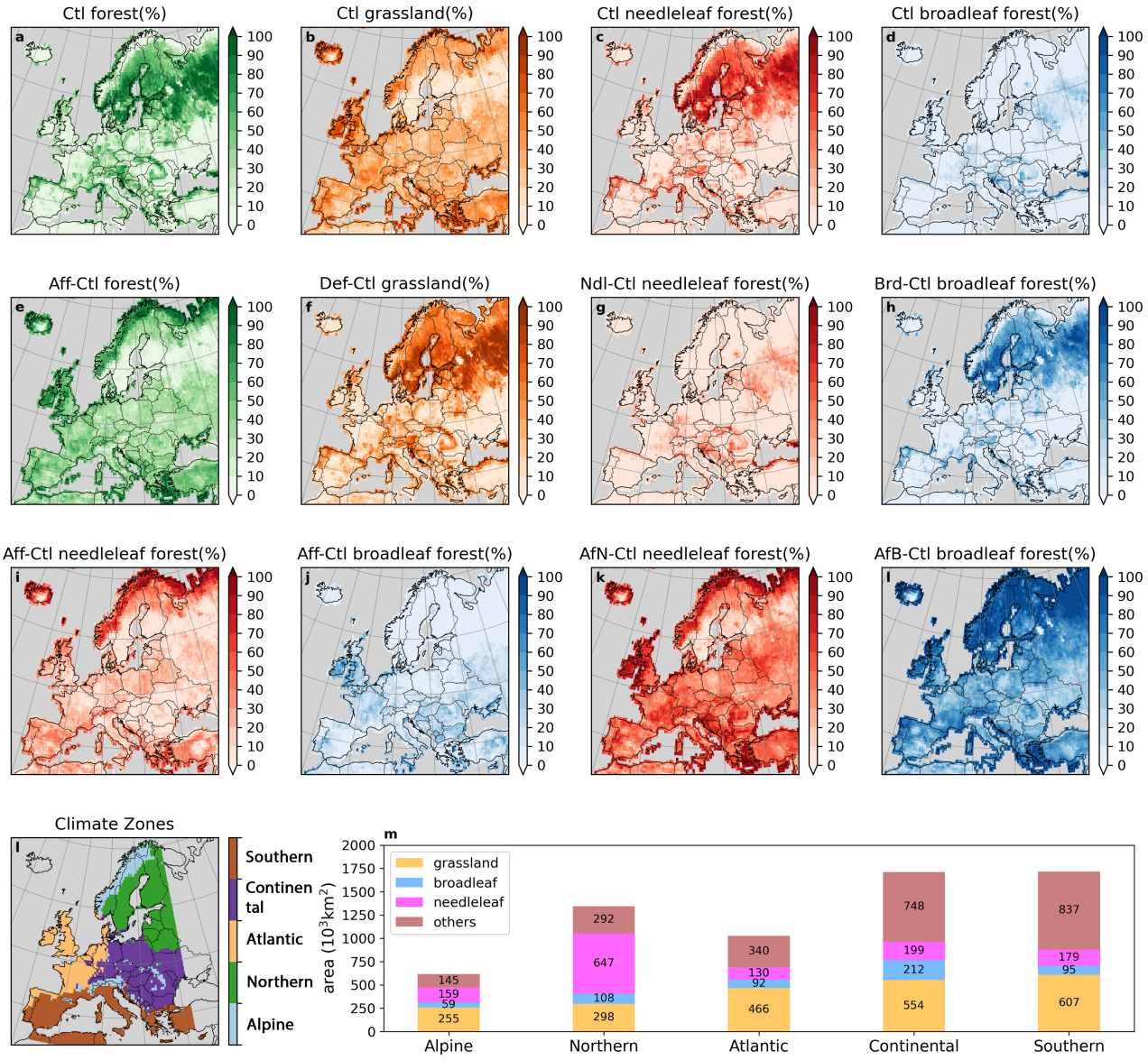

Supplementary Figure S1 | Distribution of forests, grasslands, conifer and broadleaf forests and land-use changes in idealistic scenarios. This is the supplementary figure for Figure 1 in the main text. **a-d** Present-day distribution (fraction of grid cell areas) of forests (**a**), grasslands (**b**), conifer forests (**c**), and broadleaf forests (**d**), which is used for the control (Ctl) simulation. **e-l** Changes in forests (fraction of grid cell areas) in the forestation (Aff) scenario (**e**), changes in grasslands in the deforestation (Def) scenario (**f**), changes in conifer forests in the conifer (Ndl) scenario (**g**), changes in broadleaf forests in the broadleaf (Brd) scenario (**h**), changes in conifer forests in Aff scenario (**i**), changes in broadleaf forests in Aff scenario (**j**), changes in conifer in the forestation plus conifer (AfN) scenario (**k**), and changes in broadleaf in the forestation plus broadleaf (AfB) scenario (**l**). **l** Grid cells corresponding to five climate regions (Alpine, Northern, Atlantic, Continental and Southern) used for time series analysis. **m** Present-day total areas of grasslands, conifer forests, broadleaf forests and other land use types in five regions.

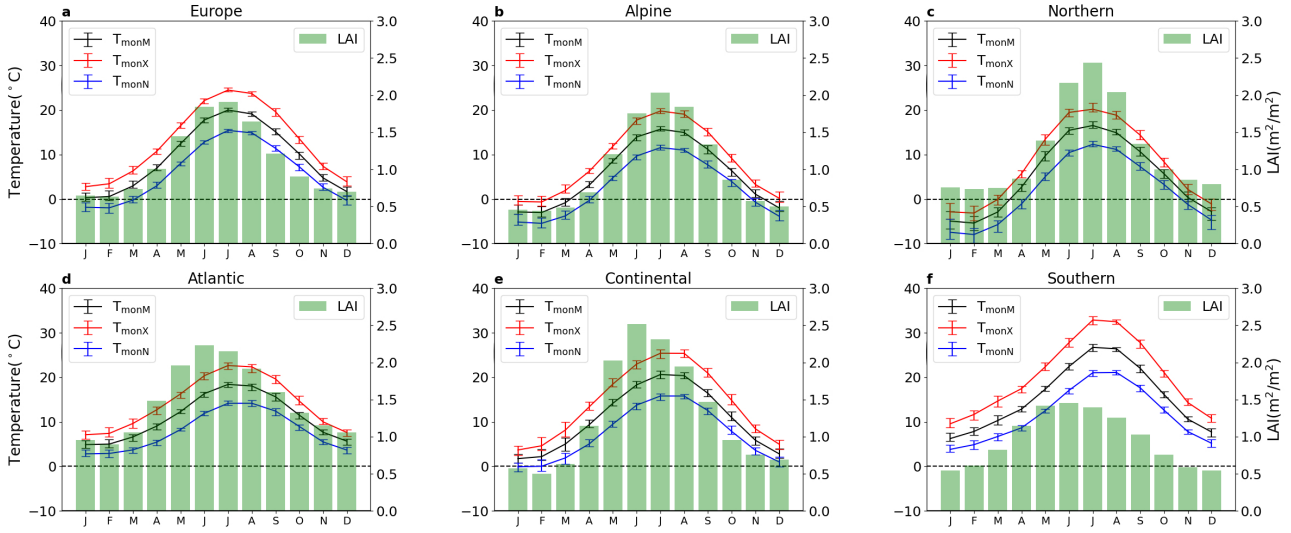

Supplementary Figure S2 | Multi-year average monthly mean leaf area index (LAI) and multi-year average monthly mean daily mean (T_{monM}), daily maximum (T_{monX}) and daili minimum (T_{monN}) in Europe (**a**) and five sub-regions (**b-f**).

2 Supplementary Notes

2.1 Supplementary Note 1: Impacts on surface properties of forest changes

Land-use changes affect several land surface properties, including leaf area index (LAI), albedo and roughness. conifer forests have the highest LAI, followed by broadleaf forests, and grasslands have the lowest (Figure S3). Higher LAI can lead to higher canopy evaporation and transpiration when water is available[1]. Albedo (for direct and visible lights) in most regions is not substantially affected by forest cover and composition change, except in high-latitude and high-altitude areas that are more likely covered in snow for extended periods, which makes local albedo more sensitive to temperature changes (Figure S4). Simulations reveal that conifer forests could substantially decrease albedo in Scandinavian mountains, while deforestation could increase it in the northern areas. Land use changes can also alter surface roughness, and the impacts are very similar for different roughness (of sensible heat or latent heat; Figure S5, S6). conifer trees have the highest roughness, while grasslands have the lowest roughness.

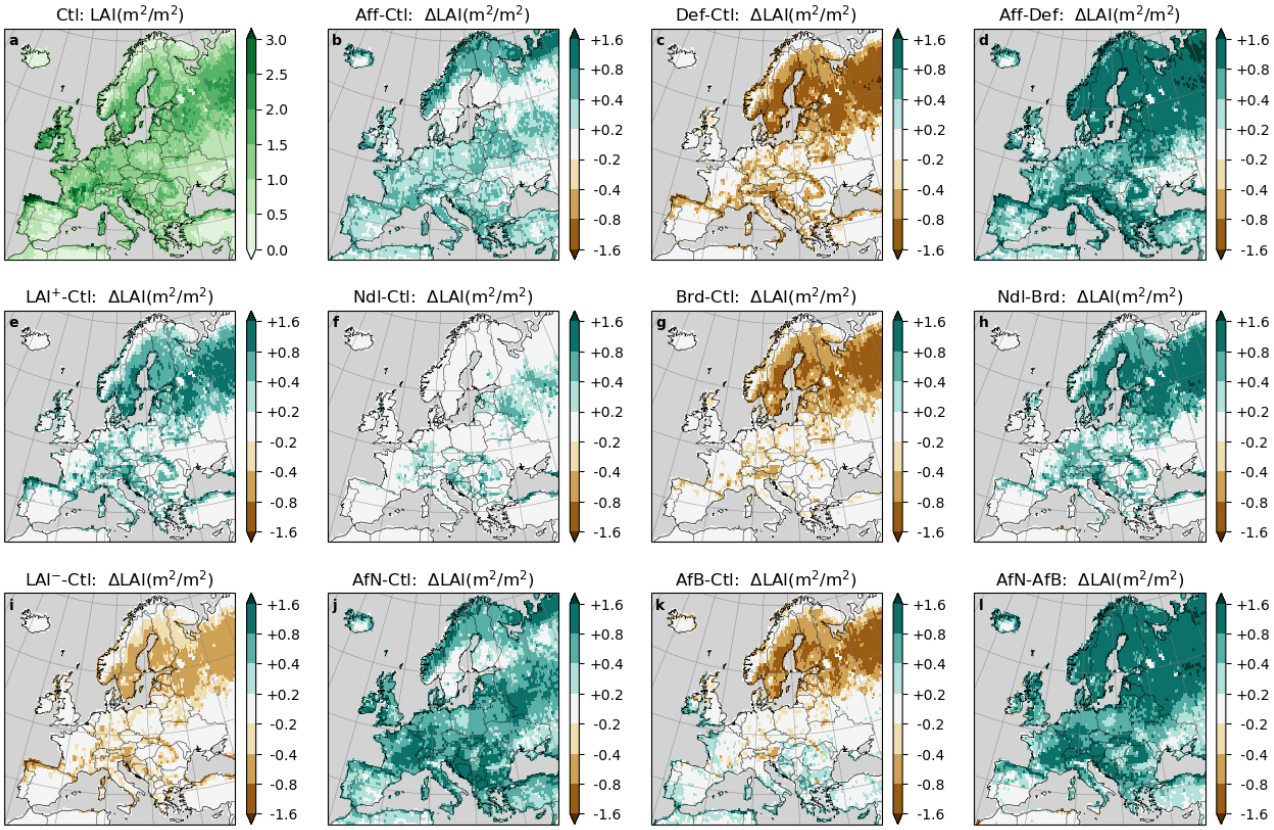

Supplementary Figure S3 | Present-day multi-year mean leaf area index (LAI) (**a**) and changes between different scenarios (**b-l**).

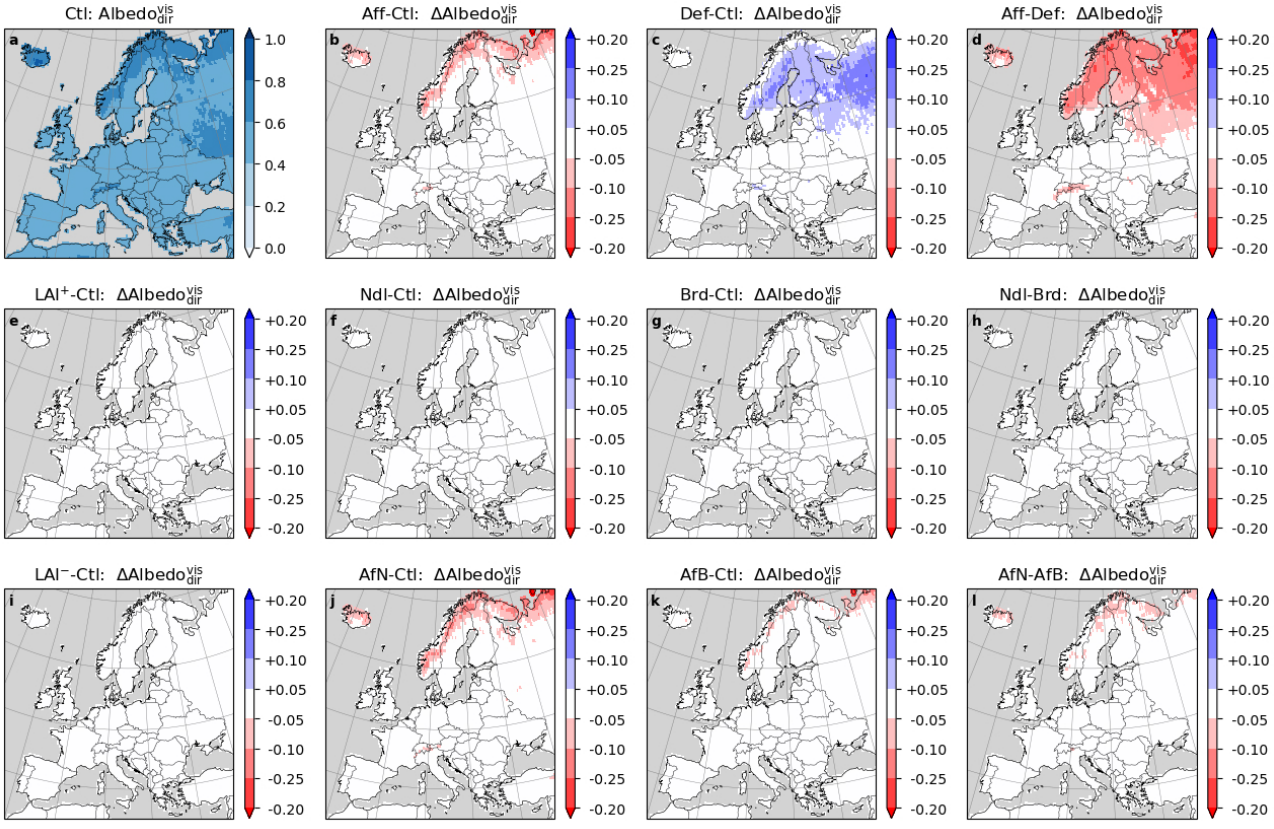

Supplementary Figure S4 | Present-day multi-year mean albedo (**a**) and changes between different scenarios (**b-l**).

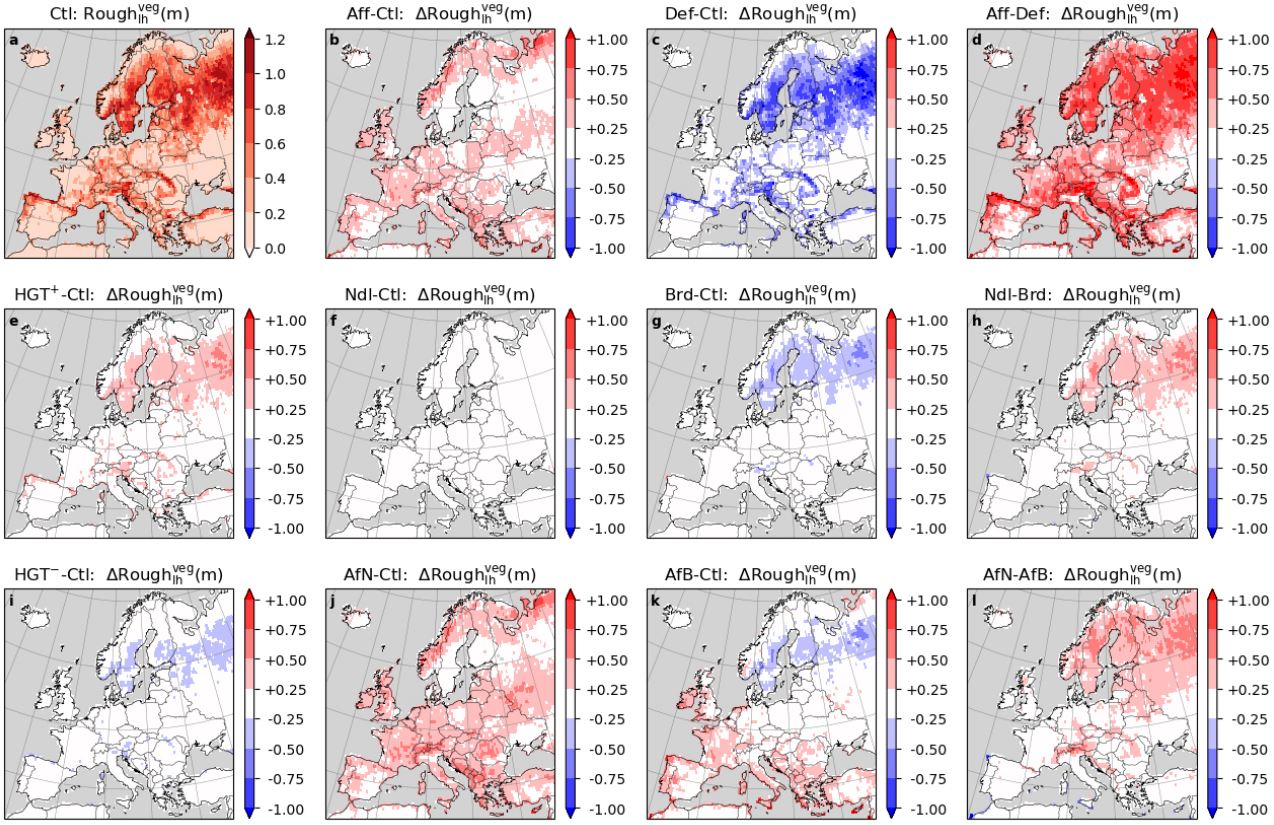

Supplementary Figure S5 | Present-day multi-year mean vegetation roughness of latent heat ($\mathrm{Rough}_{\mathrm{lh}}^{\mathrm{veg}}$) (**a**) and changes between different scenarios (**b-l**).

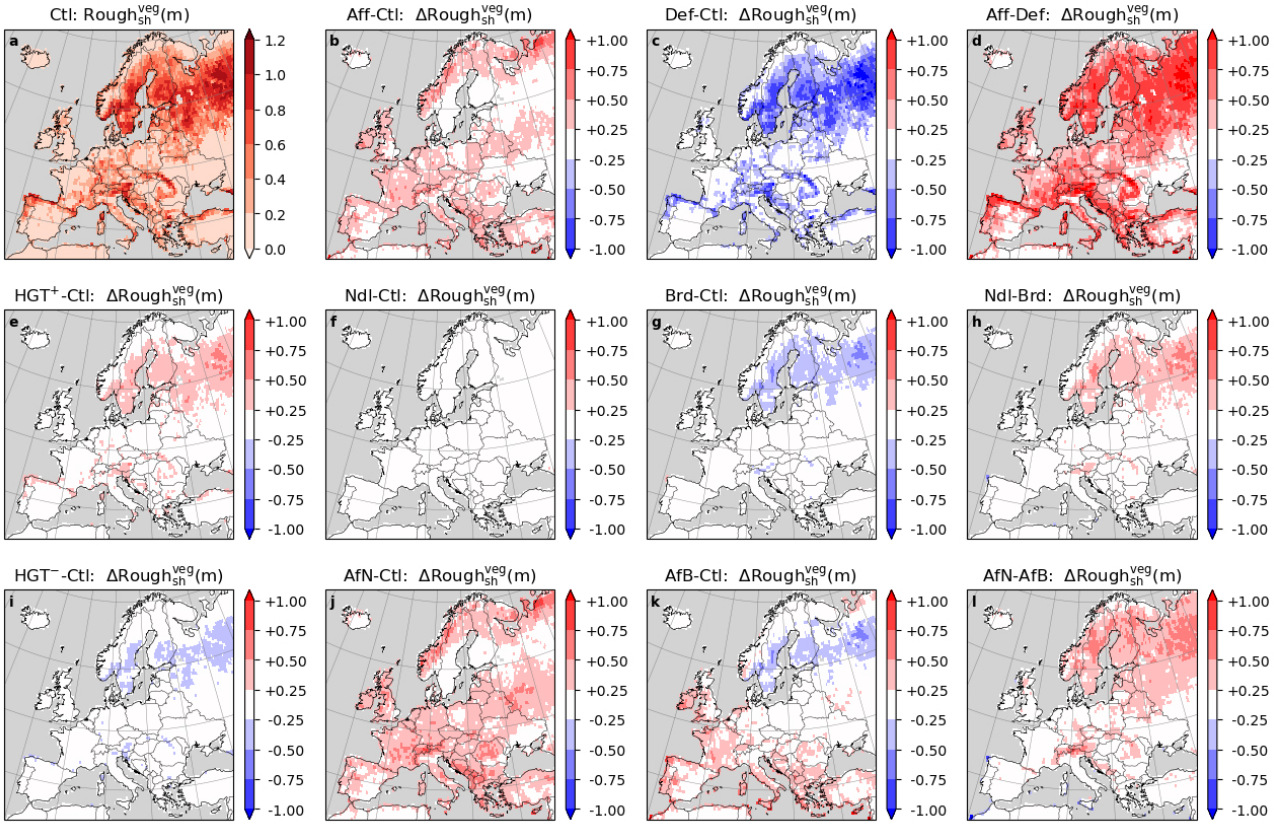

Supplementary Figure S6 | Present-day multi-year mean vegetation roughness of sensible heat ($\mathrm{Rough}_{\mathrm{sh}}^{\mathrm{veg}}$) (**a**) and changes between different scenarios (**b-l**).

2.2 Supplementary Note 2: Changes in surface energy balance caused by forestation and deforestation

In this section, we present changes in mean near-surface air temperature and surface energy balance caused by forestation and deforestation scenarios (Aff and Def in the main text).

The impacts of forestation and deforestation on multi-year annual mean 2-meter air temperature (T_{annM}) have spatial heterogeneity. Forestation warms the air in high-latitude and high-altitude areas (e.g., 0.3-0.5 °C in Scandinavian mountains), but cools it in low-latitude regions (e.g., 0.1-0.3 °C over most grid cells), with deforestation showing opposite effects (Figure S7). In high-latitude and high-altitude areas, the warming effects of forestation on multi-year mean temperature are more substantial when limited to summer and spring (T_{sumM} and T_{sprM}; Figure S7b,e,j), exceeding 0.5 and 1.0 °C in many grid cells. This is primarily because SWnet is higher in these seasons (Figure S8). In spring, despite weaker incoming energy fluxes, forestation has stronger impacts, which could be attributed to the snow masking effect of forest and pronounced albedo changes accelerated by cryospheric feedback (Figure S4b)[2]. These warming effects in spring also exist in lower-latitude and lower-altitude areas (Figure S7j), though with a smaller magnitude. However, in summer and on yearly averages (Figure S7b,f), these effects are reverse to cooling impacts due to increased LHF (Figure S9f) from higher LAI (Figure S3b). Although SHF is increased (Figure S10f), the decreased LWup still causes a lower T_{sumM}. In other words, during summer, the evaporative cooling effects of forestation will dominate the response. Notably, forestation also increases LWdown in high-latitude and high-altitude areas, with a higher magnitude in spring (Figure S12), which could be induced by increased LWup and higher water vapour concentration in the atmosphere. Although the changes in Rgnd are near 0 when averaged across the whole year, simulations show that forestation causes net positive Rgnd in spring and negative Rgnd in summer in high-latitude and high-altitude areas (Figure S13). This indicates that in spring, the energy influxes exceed the outfluxes, and vice versa in summer, which could be related to the growth of vegetation (Figure S2).

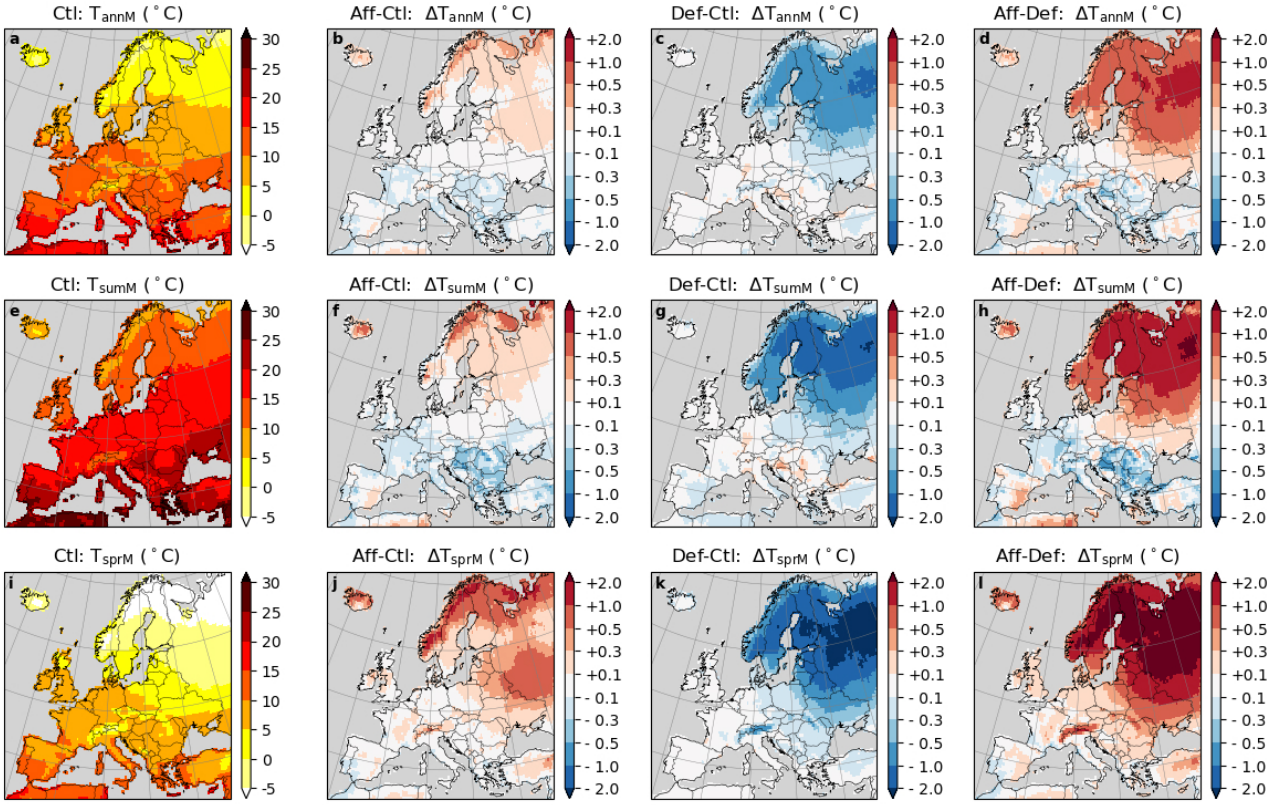

Supplementary Figure S7 | Impacts of forestation and deforestation on multi-year annual and seasonal mean 2-meter air temperature. a,e,i Multi-year (2025-2059) annual (T_{annM}: **a**), summer (T_{sumM}: **e**) and spring (T_{sprM}: **i**) mean 2-meter air temperature simulated by the control (Ctl) simulation. **b,f,j** Difference in T_{annM} (**b**), T_{sumM} (**f**) and T_{sprM} **j** between simulations with the forestation scenario (Aff) and Ctl (Aff minus Ctl). **c,g,k** Difference in T_{annM} (**c**), T_{sumM} (**g**) and T_{sprM} **k** between simulations with the deforestation scenario (Def) and Ctl (Def minus Ctl). **d,h,l** Difference in T_{annM} (**d**), T_{sumM} (**h**) and T_{sprM} **l** between Aff and Def (Aff minus Def).

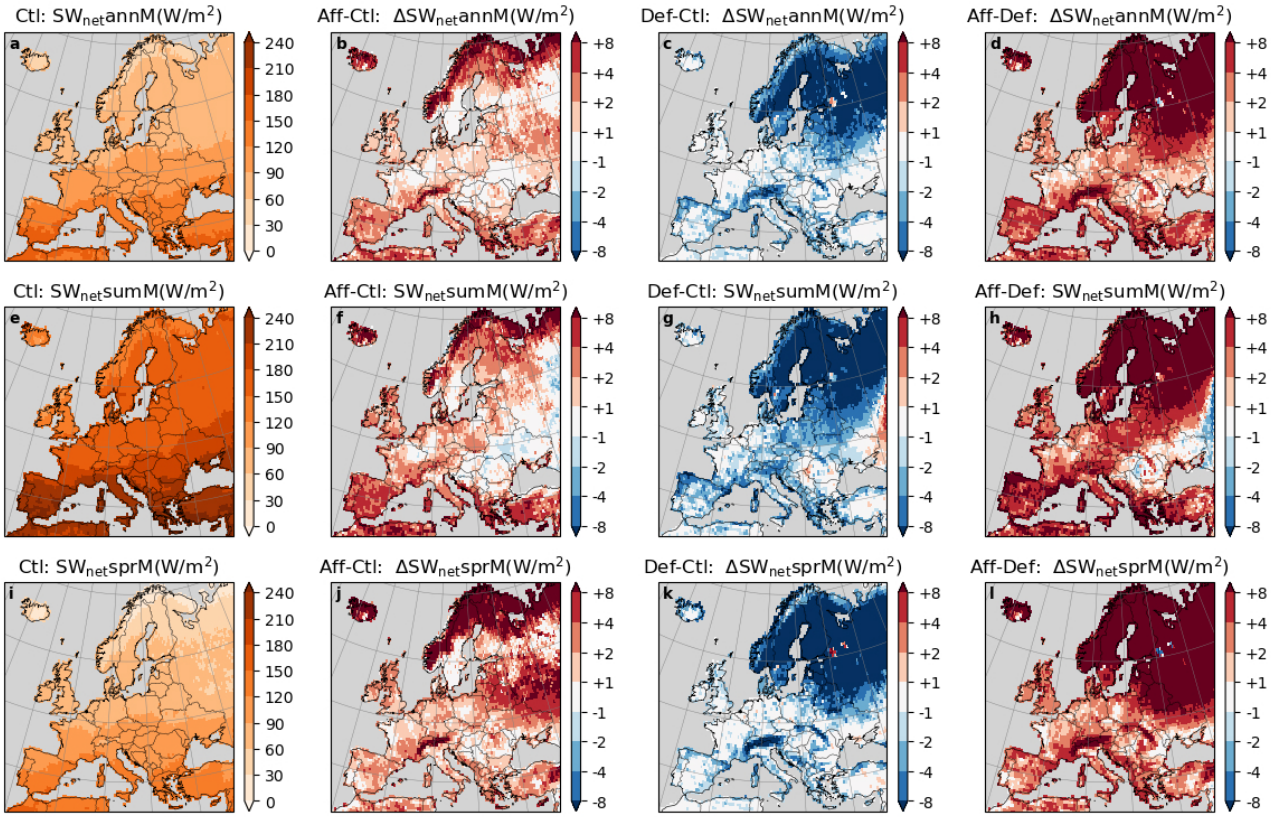

Supplementary Figure S8 | **a,e,i** Multi-year (2025-2059) annual ($SWnet_{annM}$: **a**), summer ($SWnet_{sumM}$: **e**) and spring ($SWnet_{sprM}$: **i**) mean net downwelling shortwave radiation simulated by the control (Ctl) simulation. **b,f,j** Difference in $SWnet_{annM}$ (**b**), $SWnet_{sumM}$ (**f**) and $SWnet_{sprM}$ **j** between simulations with the forestation scenario (Aff) and Ctl (Aff minus Ctl). **c,g,k** Difference in $SWnet_{annM}$ (**c**), $SWnet_{sumM}$ (**g**) and $SWnet_{sprM}$ **k** between simulations with the deforestation scenario (Def) and Ctl (Def minus Ctl). **d,h,l** Difference in $SWnet_{annM}$ (**d**), $SWnet_{sumM}$ (**h**) and $SWnet_{sprM}$ **l** between Aff and Def (Aff minus Def).

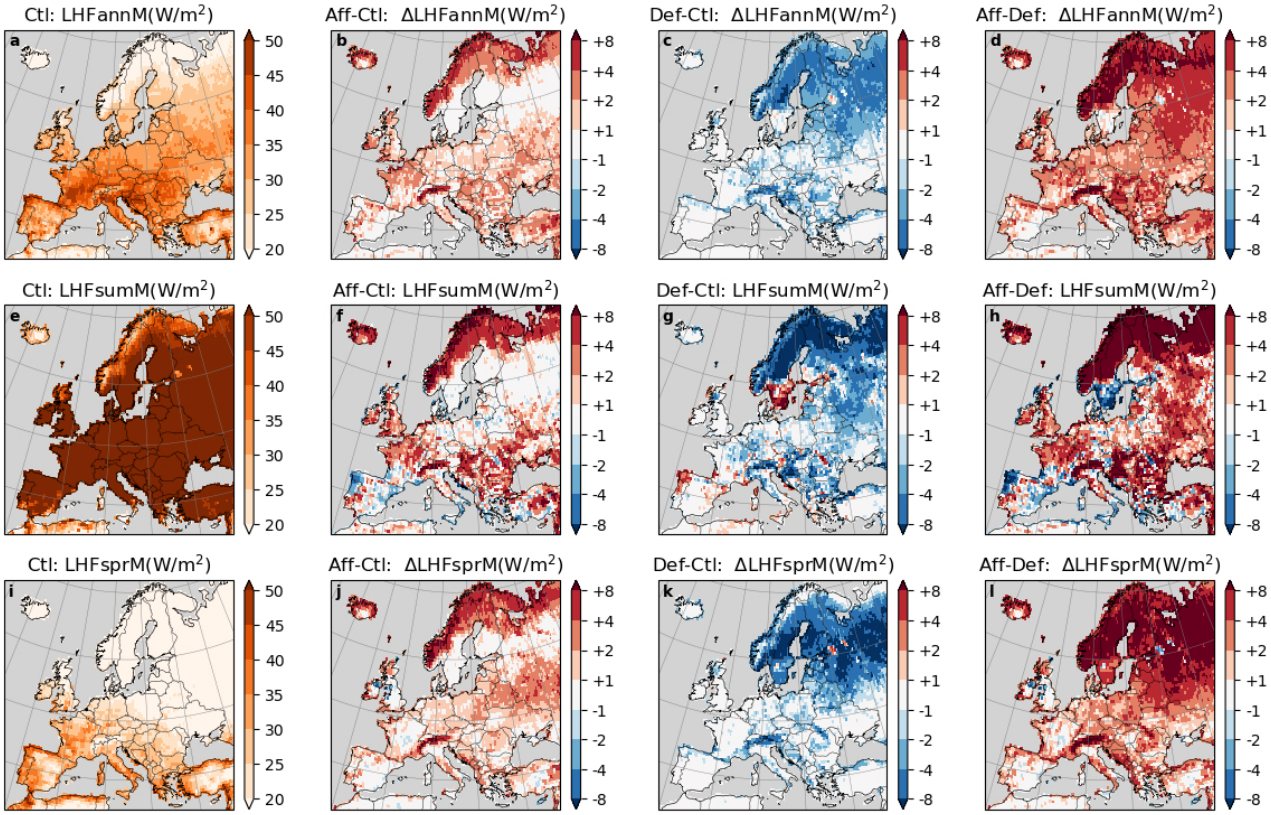

Supplementary Figure S9 | Same as Figure S8 but for Latent Heat Flux (LHF).

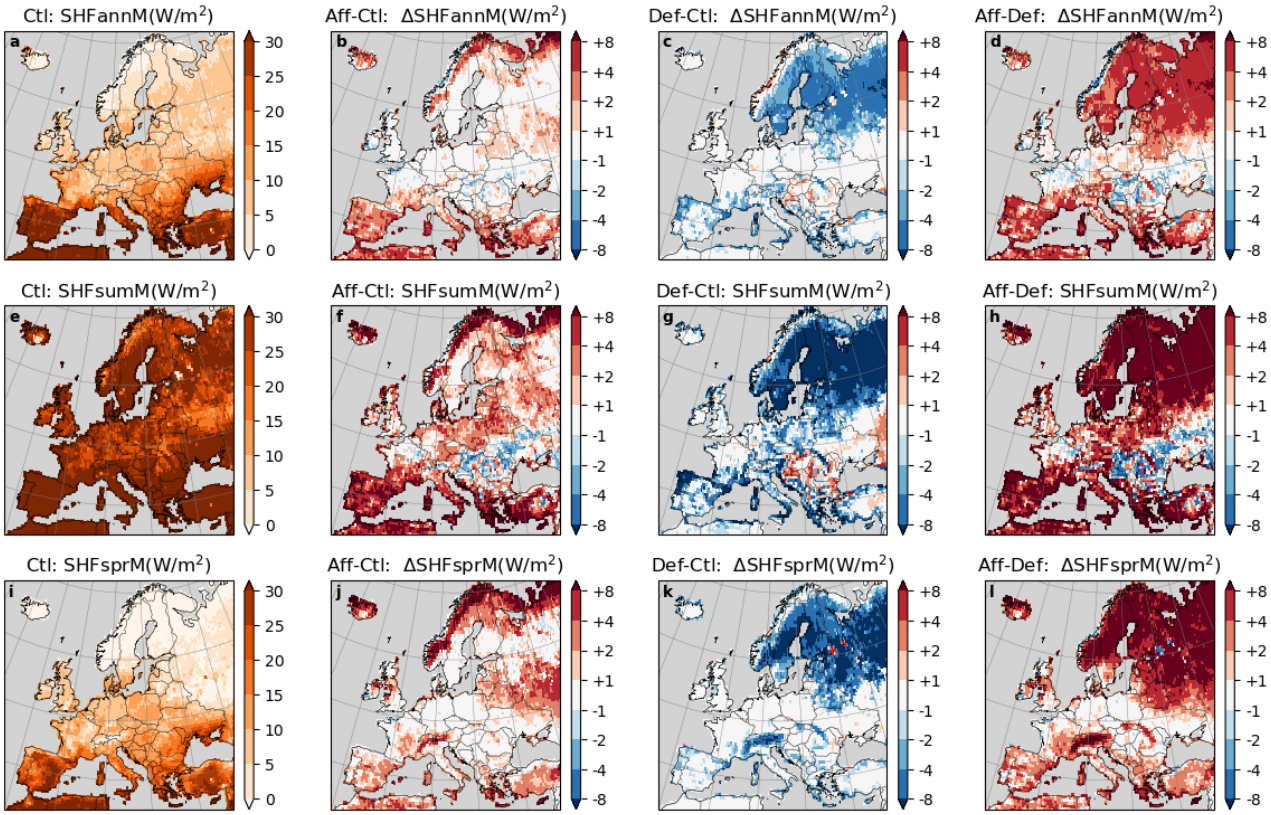

Supplementary Figure S10 | Same as Figure S8 but for Sensible Heat Flux (SHF).

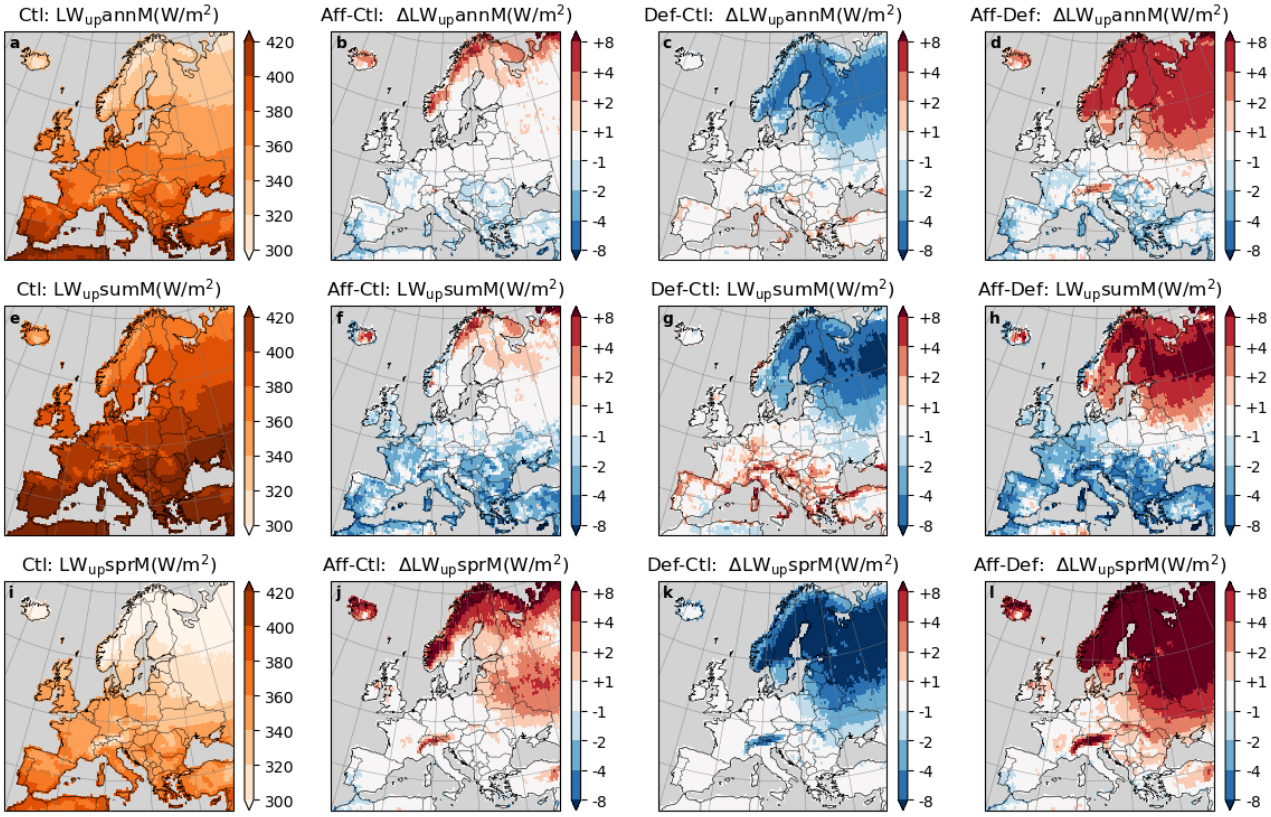

Supplementary Figure S11 | Same as Figure S8 but for upwelling longwave radiation (LWup).

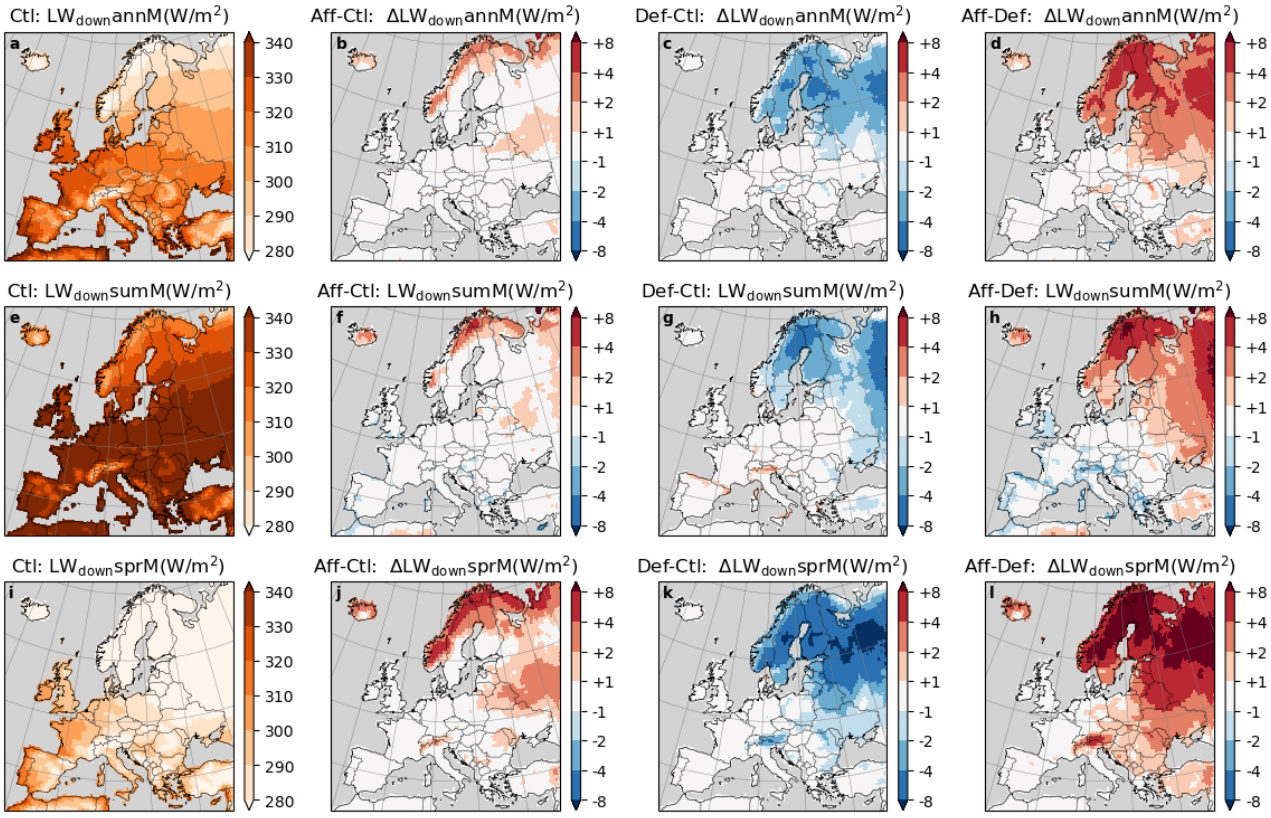

Supplementary Figure S12 | Same as Figure S8 but for downwelling longwave radiation (LWdown).

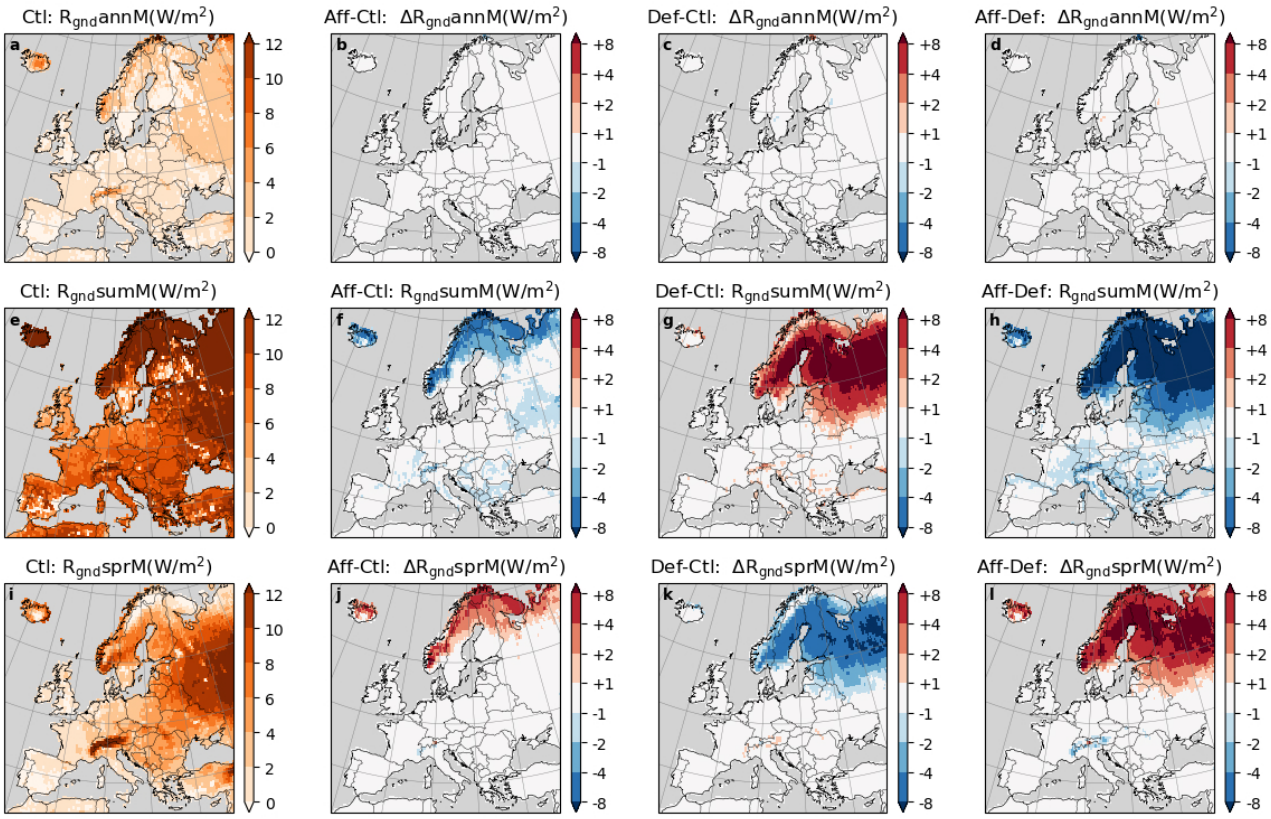

Supplementary Figure S13 | Same as Figure S8 but for ground heat flux (Rgnd).

Changes in T_{monM} confirm the spatial and temporal variance in biogeophysical impacts of forestation and deforestation (Figure S14a,d,g,j,m). In the Alpine and Northern regions, the peak occurs from March to May, when forestation could induce a ∼0.7 and ∼0.5 °C of warming and deforestation could lead to a ∼0.8 and ∼1.9 °C of cooling, respectively (Figure S14a,d). In these two regions, forestation causes an increase in both LWup and SHF, and deforestation decreases them, which is mainly triggered by changes in SWnet, despite the counter effects from LHF (Figure S15a-d). In other regions, the impacts of forestation-deforestation are smaller and fluctuate around 0. For example, in the Continental region, forestation results in a cooling of ∼0.3 °C in August, and a warming of ∼0.2 °C in March, while deforestation leads to a cooling of ∼0.4 °C in April, and a warming of ∼0.1 °C in August. The reasons include the relatively smaller modifications in land use (Figure S1), and the opposite signals in changes in LWup and SHF in most cases (Figure S14g,j,m), as in these regions, forests generally generate a relatively larger increase in LHF during the summer, which masks the increase in SWnet (Figure S15e-j).

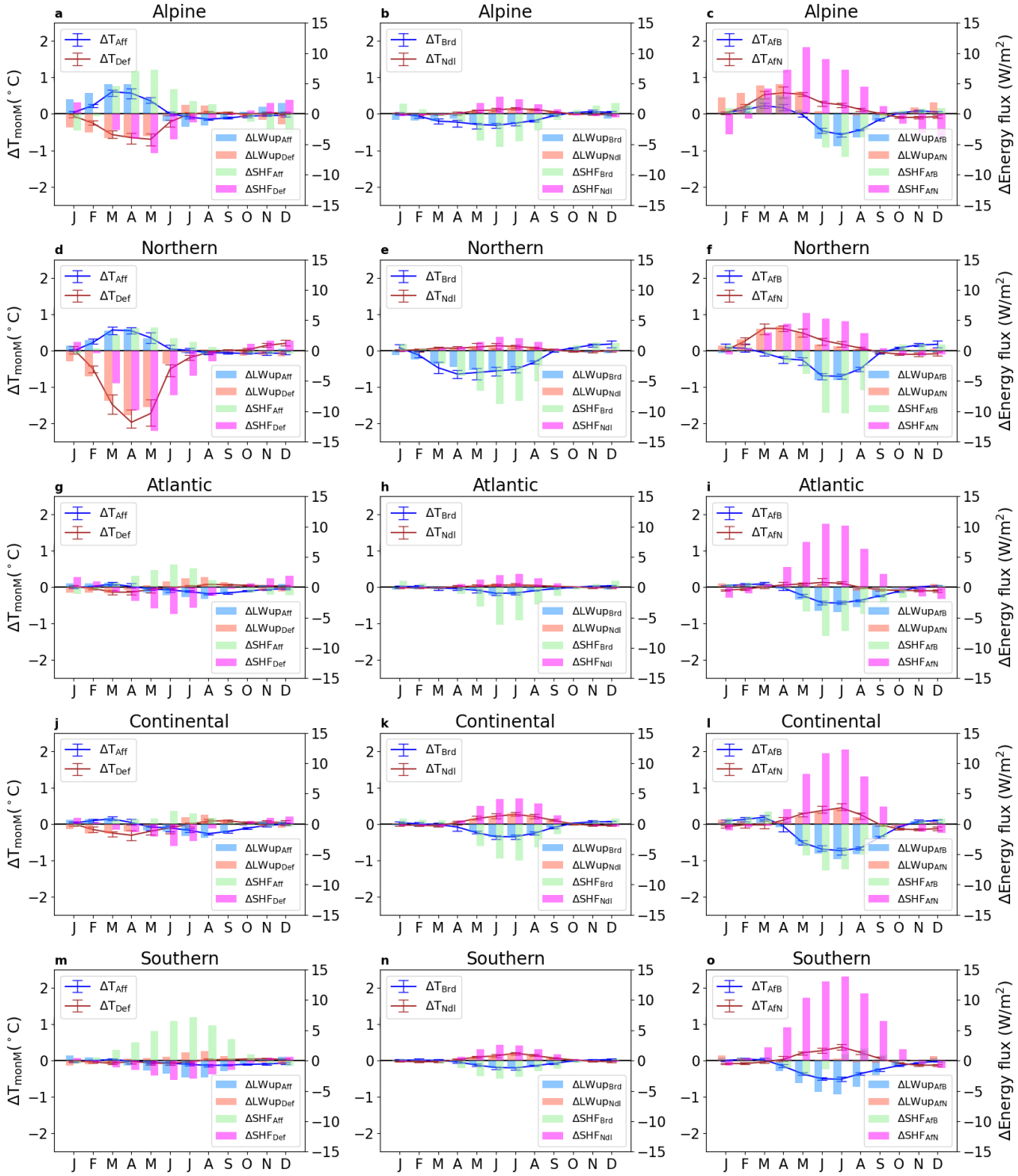

Supplementary Figure S14 | Seasonal pattern of forest-induced biogeophysical impacts across different regions. Changes in multi-year mean monthly mean daily mean temperature (T_{monM}), upwelling longwave radiation (LWup), and sensible heat flux (SHF) induced by forestation-deforestation (Aff-Def: **left column**), conifer-broadleaf (Ndl-Brd: **mid column**), and forestation plus conifer-broadleaf (AfN-AfB: **right column**) averaged over five regions: Alpine (**a-c**), Northern (**d-f**), Atlantic (**g-i**), Continental (**j-l**), and Southern (**m-o**).

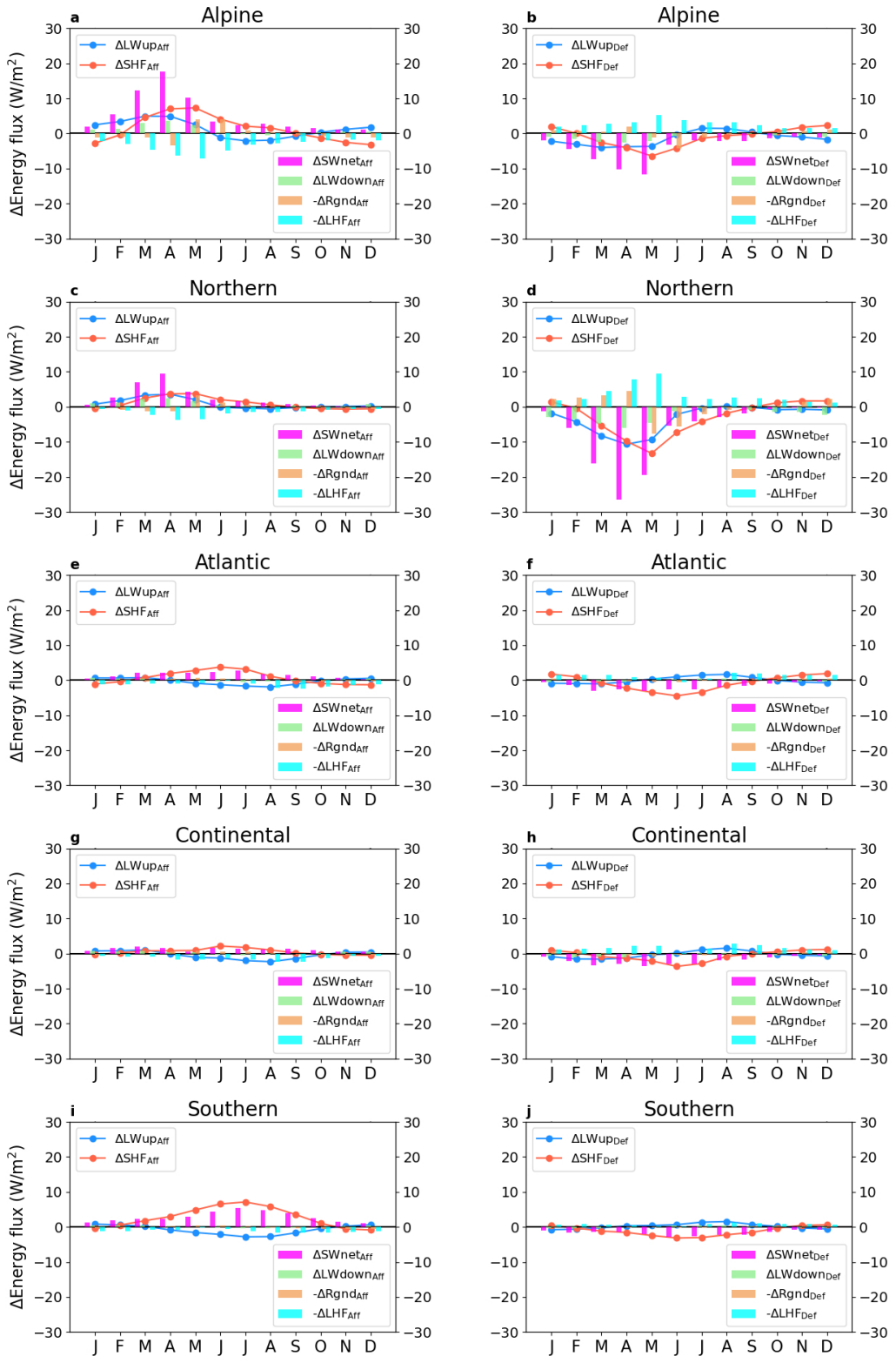

Supplementary Figure S15 | Changes in multi-year average monthly mean upwelling longwave radiation (LWup), sensible heat flux (SHF), and the contribution of other components, including net shortwave radiation (SWnet), downwelling longwave radiation (LWdown), ground heat flux (Rgnd), and latent heat flux (LHF), induced by forestation (Aff) and deforestation (Def).

2.3 Supplementary Note 3: Changes in surface energy balance of other forest changes

In this section, we present changes in mean near-surface air temperature and surface energy balance caused by transitions in forest types (Brd and Ndl in the main text) and the combining changes of forestation and transitions in forest types (AfB and AfN in the main text).

Switching all conifer forests to broadleaf decreases T_{annM}, especially over North Europe, with the magnitude more pronounced in summer ($\geq$1.0 °C in some areas) and spring ($\geq$0.5 °C in most areas) (Figure S16a,d,g). Oppositely, switching all broadleaf forests to conifer increases the temperature, though with a smaller magnitude, with summer being the most influenced season ($\geq$0.5 °C in Balkan Peninsula) (Figure S16b,e,h). The spatial pattern and magnitudes of these impacts are highly related to the changes in land use (Figure S1g,h). The cooling caused by broadleaf forests on T_{annM} and T_{sumM} result from combined effects of decreased SWnet and increased LHF (Figure S17a,d, S18a,d), which decrease both LWup and SHF (Figure S19, S20).

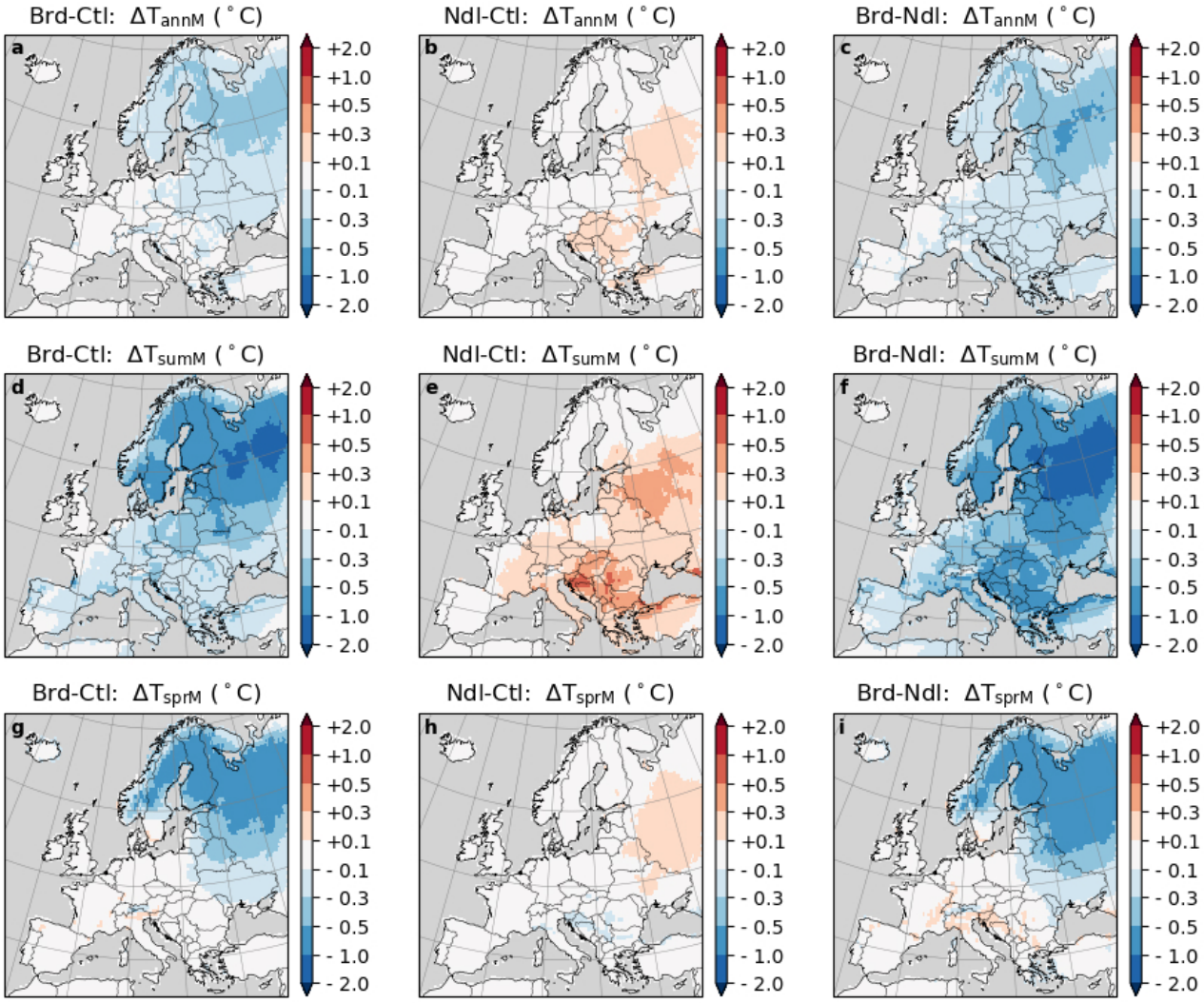

Supplementary Figure S16 | Same as Figure S7 but for the broadleaf (Brd) and conifer (Ndl) scenarios.

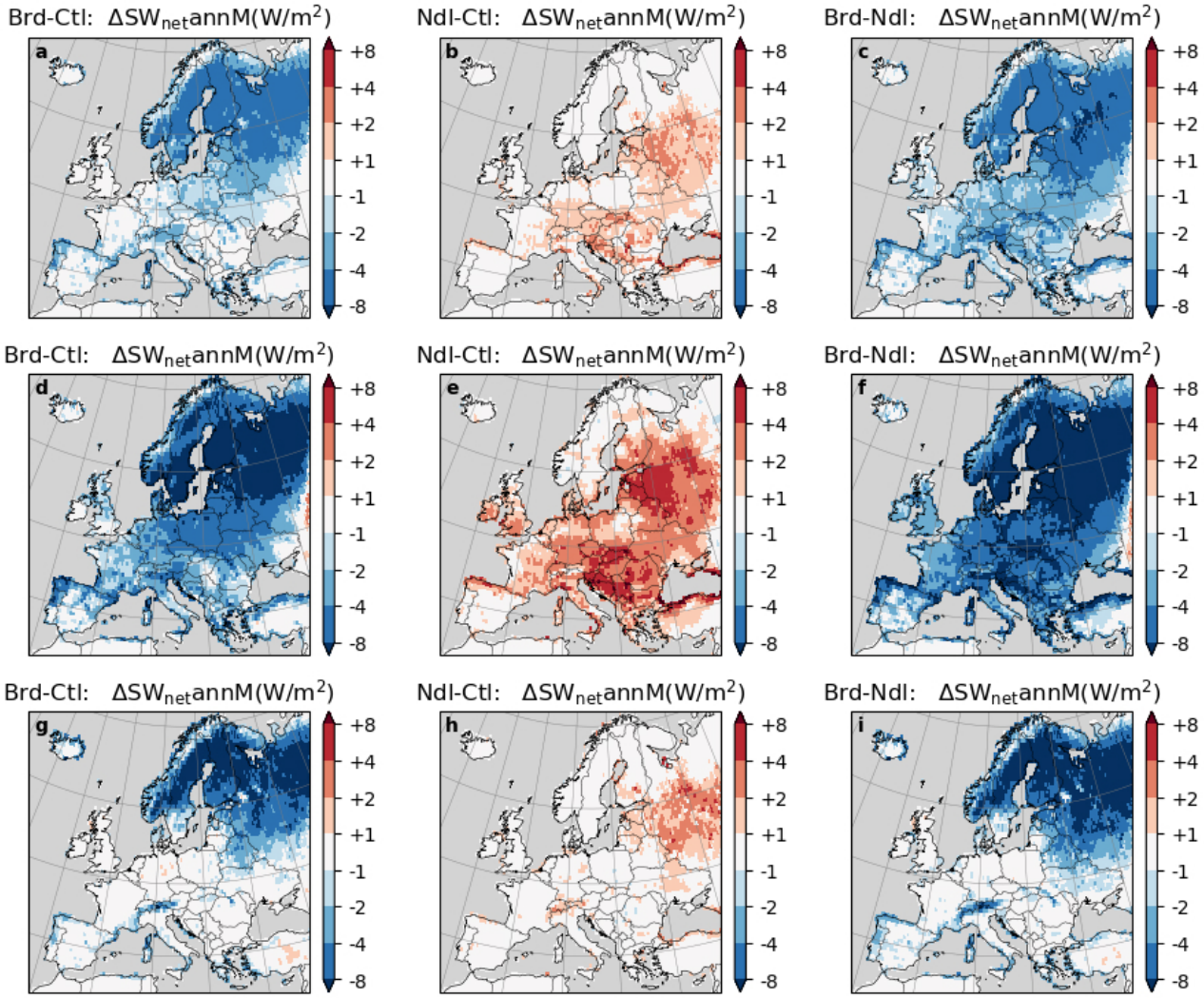

Supplementary Figure S17 | **a,d,g** Difference in $SWnet_{annM}$ (**a**), $SWnet_{sumM}$ (**d**) and $SWnet_{sprM}$ **g** between simulations with the broadleaf scenario (Brd) and Ctl (Brd minus Ctl). **b,e,h** Difference in $SWnet_{annM}$ (**b**), $SWnet_{sumM}$ (**e**) and $SWnet_{sprM}$ **h** between simulations with the conifer scenario (Ndl) and Ctl (Ndl minus Ctl). **c,f,i** Difference in $SWnet_{annM}$ (**c**), $SWnet_{sumM}$ (**f**) and $SWnet_{sprM}$ **i** between Brd and Ndl (Brd minus Ndl).

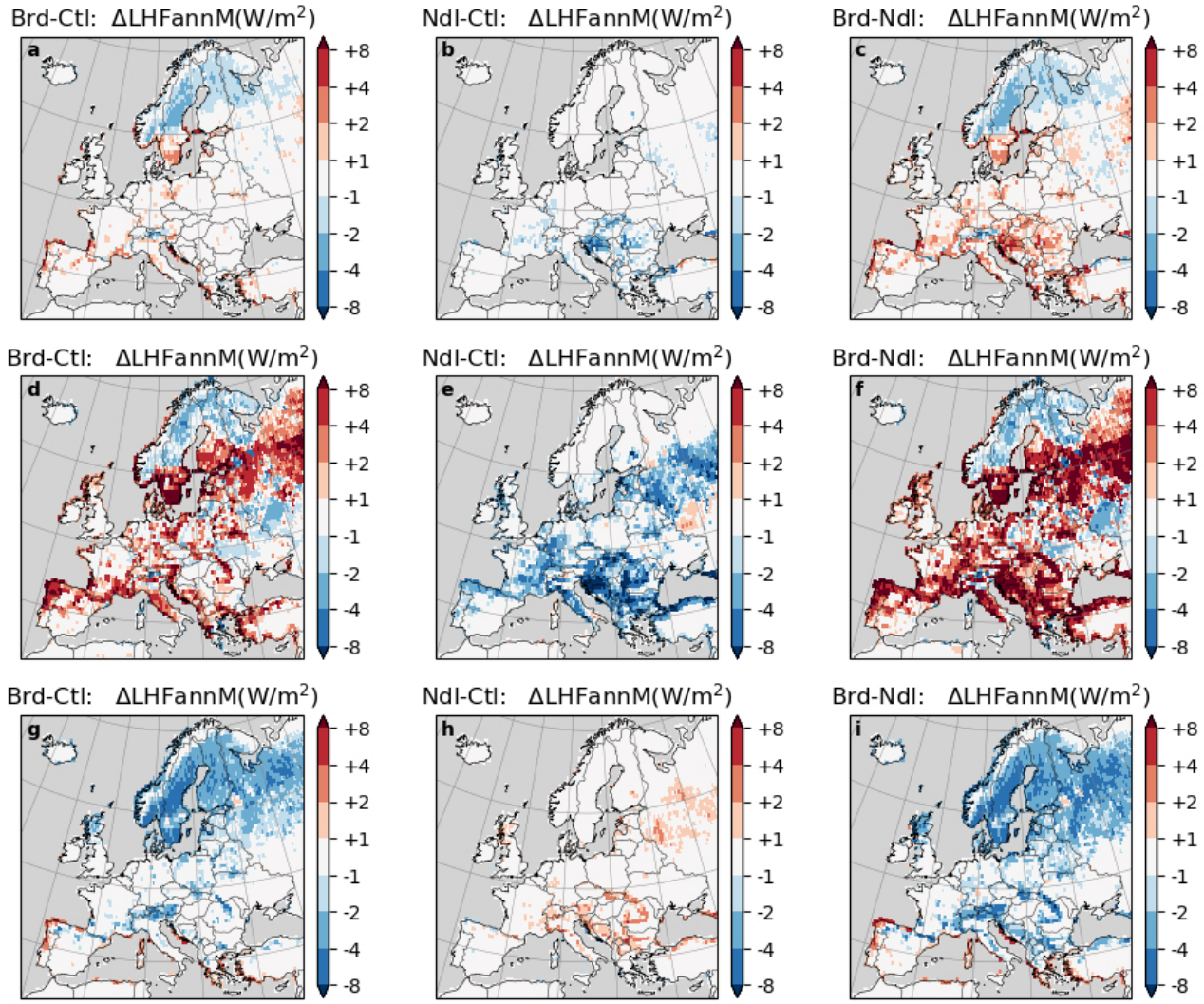

Supplementary Figure S18 | Same as Figure S17 but for Latent Heat Flux (LHF).

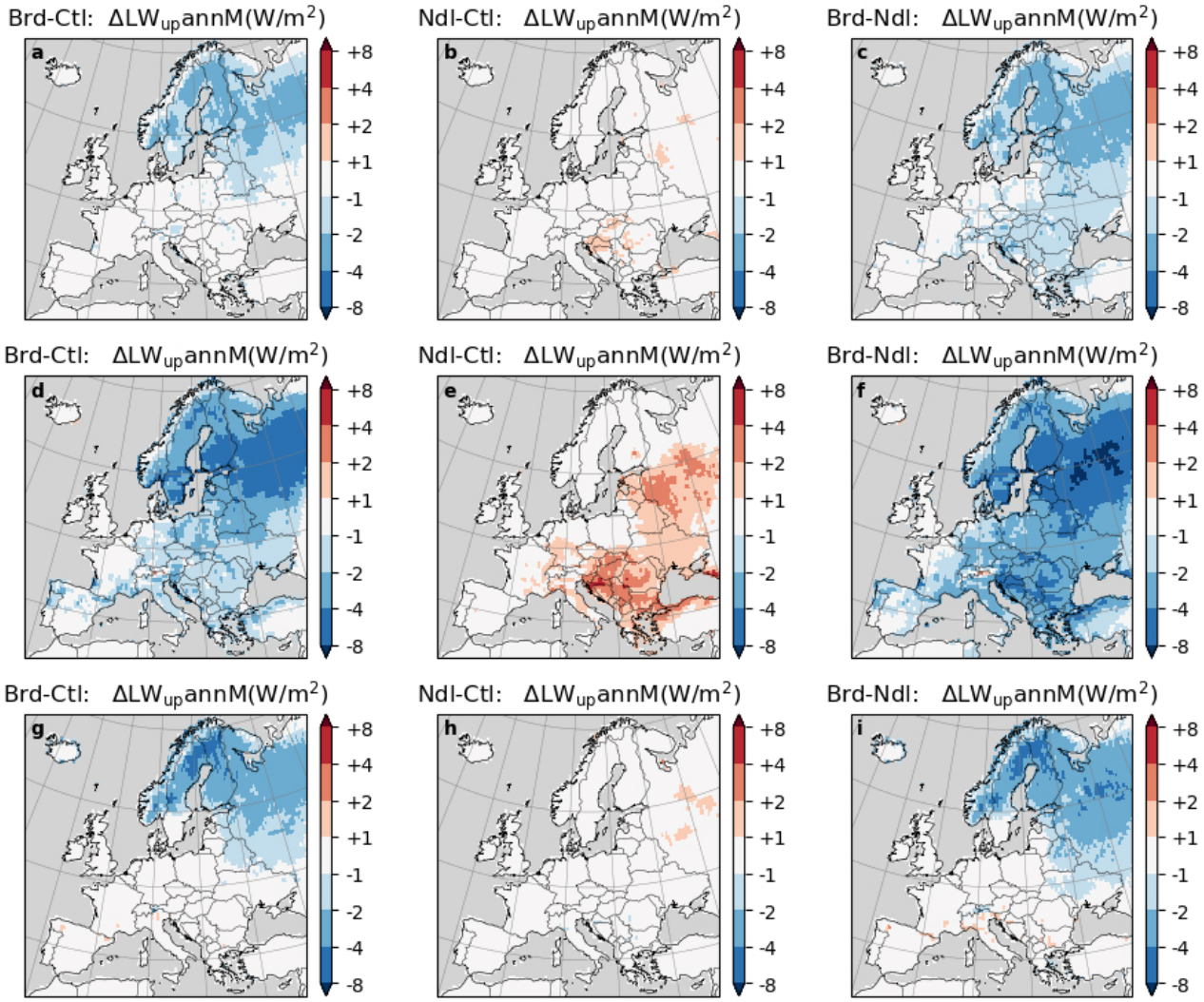

Supplementary Figure S19 | Same as Figure S17 but for upwelling longwave radiation (LWup).

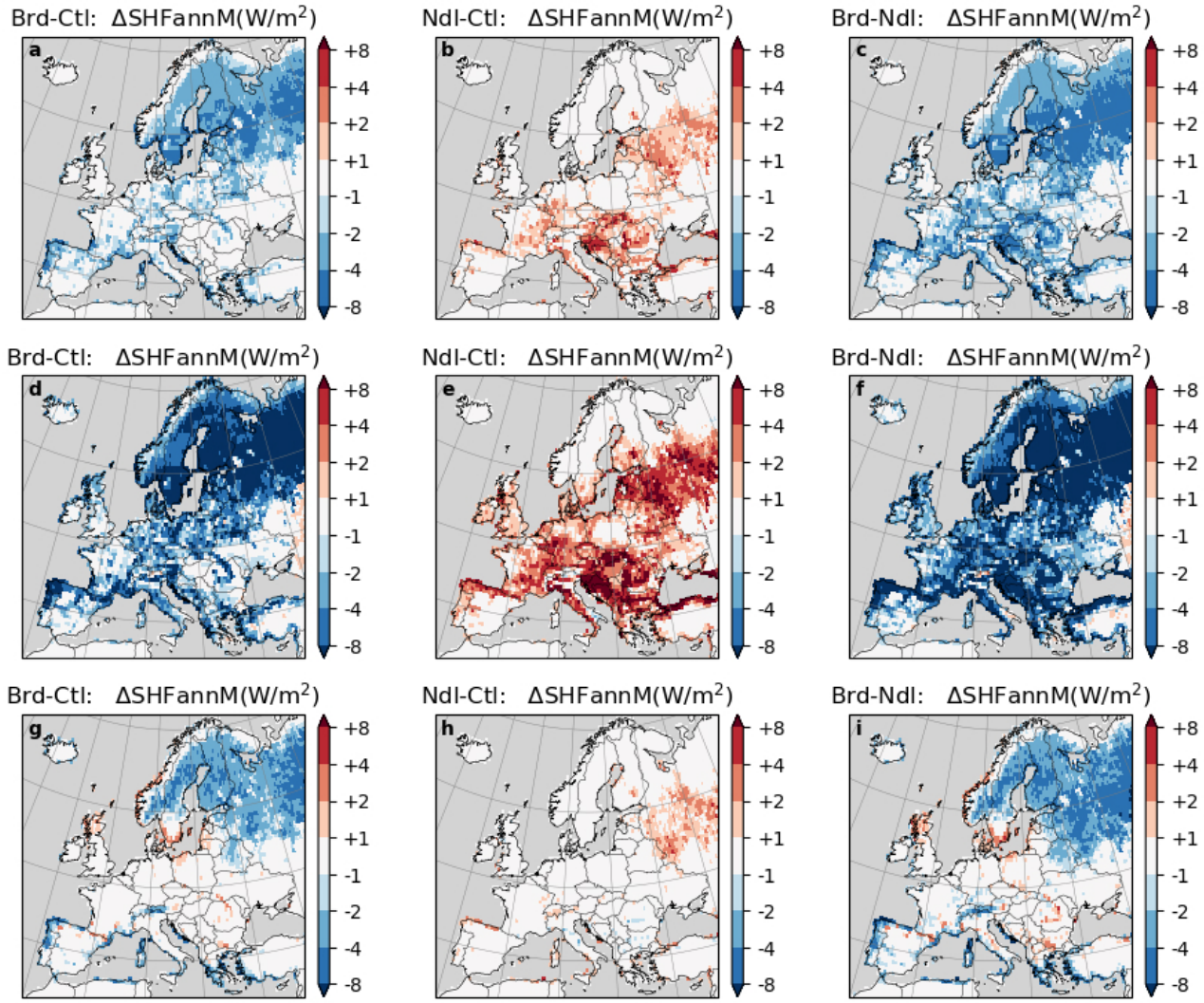

Supplementary Figure S20 | Same as Figure S17 but for Sensible Heat Flux (SHF).

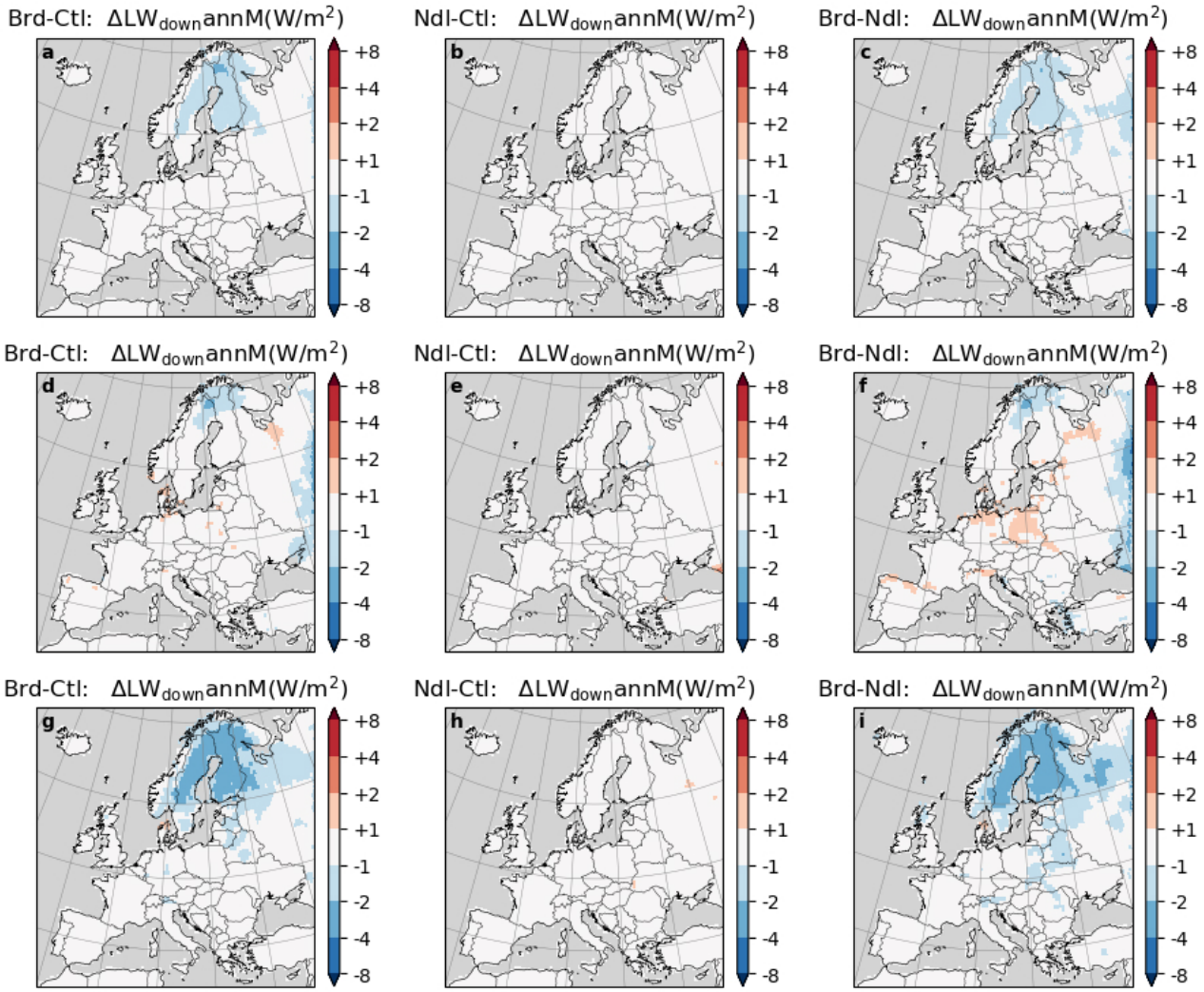

Supplementary Figure S21 | Same as Figure S17 but for downwelling longwave radiation (LWdown).

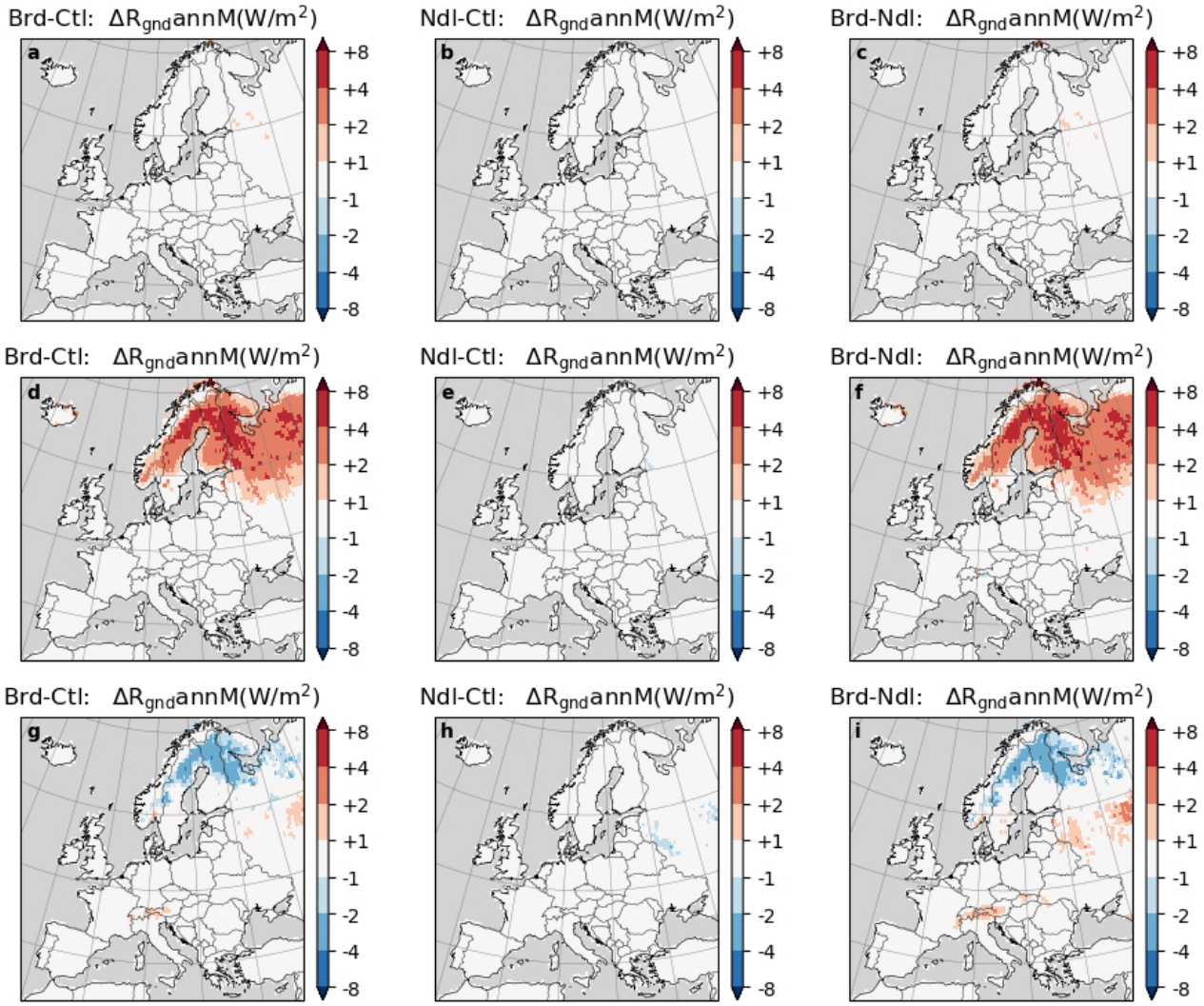

Supplementary Figure S22 | Same as Figure S17 but for ground heat flux (Rgnd).

Broadleaf/conifer forest conversion generally changes multi-year average LWup and SHF in the same direction (Figure S14b,e,h,k,n), with SWnet and LHF being the two relative largest contributors (Figure S23). In the Alpine and Northern regions, the highest impacts occur in May (broadleaf forests reduce T_{annM} by ∼0.3 °C and ∼0.7 °C, while in other regions, the peak month is July or August. The impacts on T_{annX}, T_{sumX}, T_{sprX}, T_{annN}, T_{sumN}, and T_{sprN} show similar spatial patterns, but with larger magnitude on maximum and a smaller magnitude on minimum temperature (Figure S24, S25).

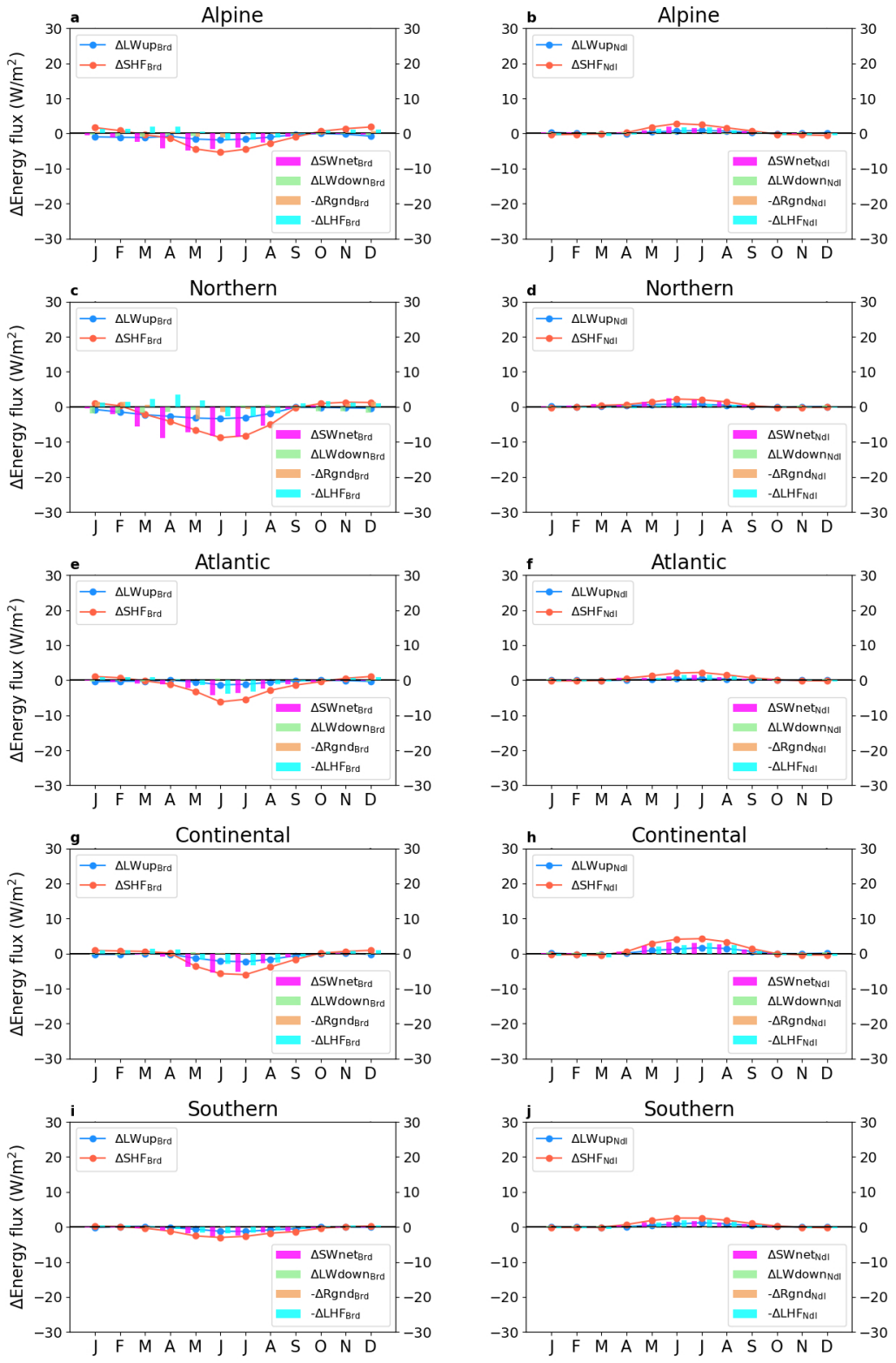

Supplementary Figure S23 | Changes in multi-year average monthly mean upwelling longwave radiation (LWup), sensible heat flux (SHF), and the contribution of other components, including net shortwave radiation (SWnet), downwelling longwave radiation (LWdown), ground heat flux (Rgnd), and latent heat flux (LHF), induced by broadleaf (Brd) and conifer (Ndl) scenarios.

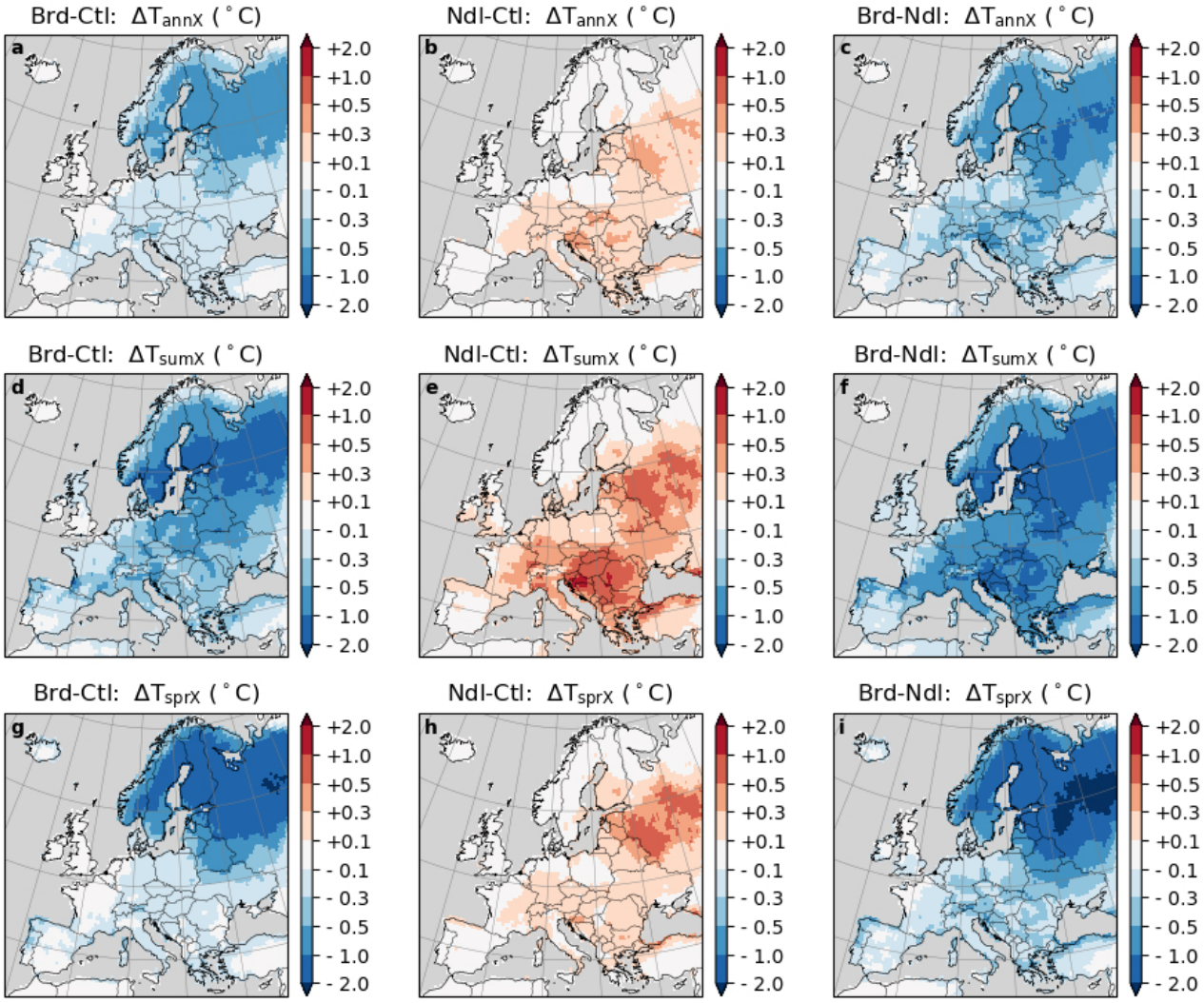

Supplementary Figure S24 | Same as Figure S16 but for multi-year average monthly mean daily maximum (T_{monX}).

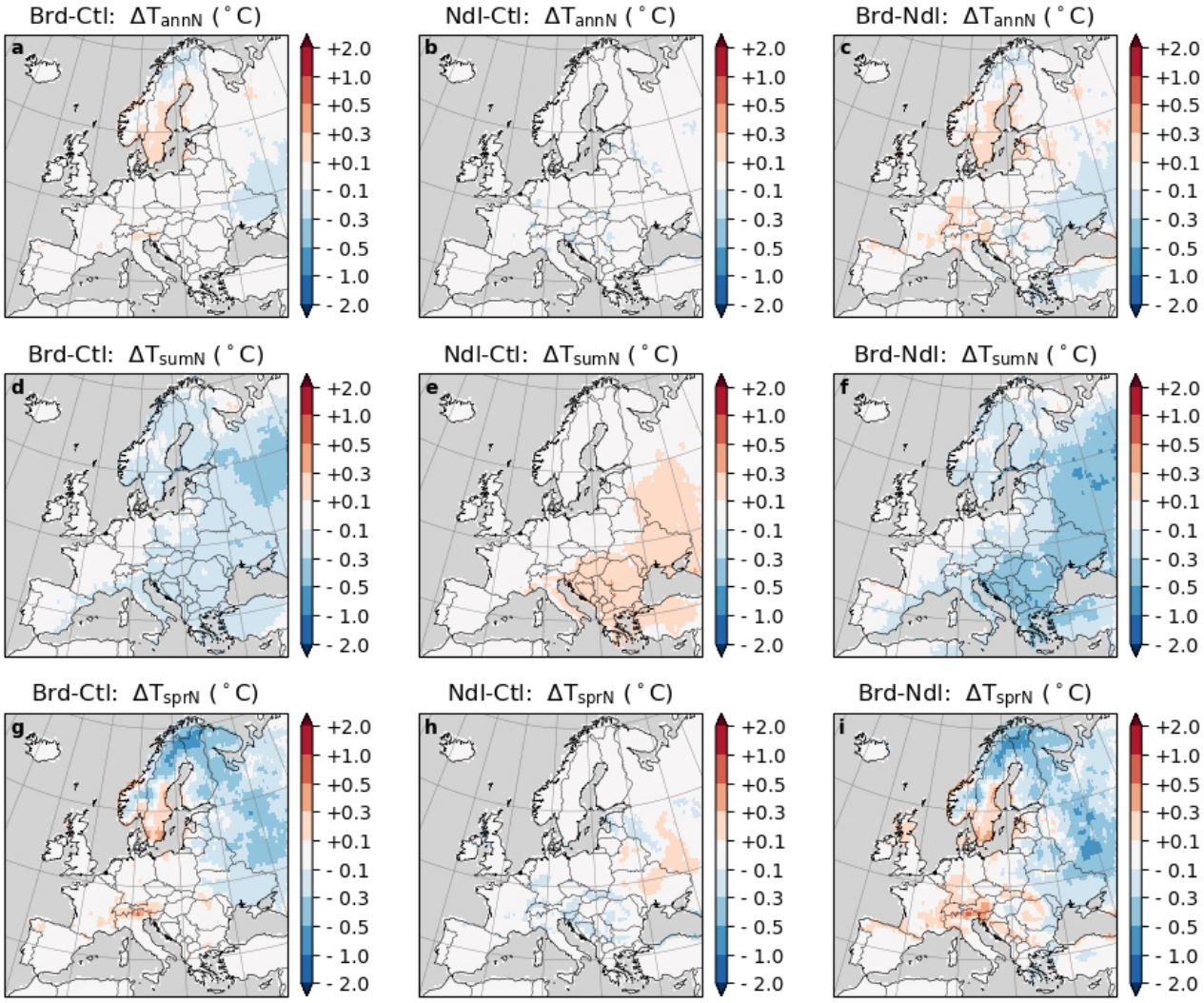

Supplementary Figure S25 | Same as Figure S16 but for multi-year average monthly mean daily minimum (T_{monN}).

Combining the forestation and broad-/conifer scenarios (AfB and AfN), leads to more substantial changes in T_{annM}, T_{sumM} and T_{sprM} (Figure S26). Under AfB scenario, T_{annM} and T_{sumM} increase over the Scandinavian mountains, but decrease over other regions. Under AfN scenario, these temperatures increase across all of Europe. The warming effects of AfN are mainly caused by increased SWnet (Figure S27b,e,h), and the cooling impacts of AfB result from the increase in LHF and decrease in SWnet (Figure S28a,d,g, S27a,d,g). AfB and AfN-induced changes in T_{monM}, LWup and SHF show various seasonal patterns among regions (Figure S14c,f,i,l,o). In Alpine regions, AfB slightly increases T_{monM} in all seasons (up to 0.3 °C) except in summer (reaching ∼0.6 °C in July), while AfN increases T_{monM} over most months (peaking at ∼0.6 °C in April). In the Northern region, AfB has cooling impacts over a longer period (March-October, with the maximum magnitude of ∼0.8 °C). In the other three regions, temperature changes induced by AfB and AfN both peak during the summer season (e.g., AfB decreases T_{monM} by around 0.5, 0.8, and 0.5 °C, respectively). This occurs because their impacts on LWup and SHF have the same signal only over a limited time in the year, while during the rest of the year, their changes mask each other. These changes are mainly induced by SWnet and LHF (Figure S33).

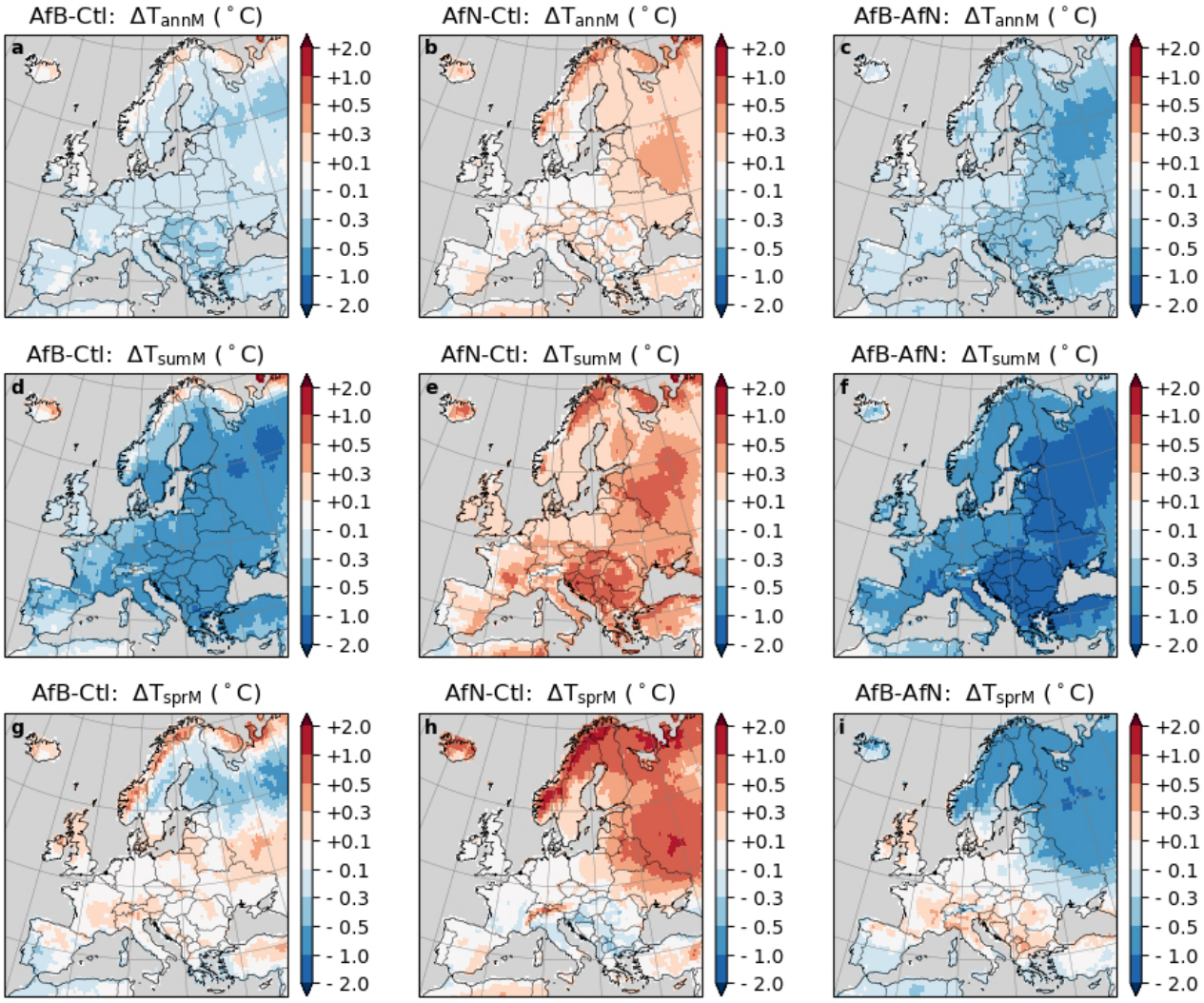

Supplementary Figure S26 | Same as Figure S7 but for the combining scenario of forestation and broadleaf (AfB) or conifer (AfN).

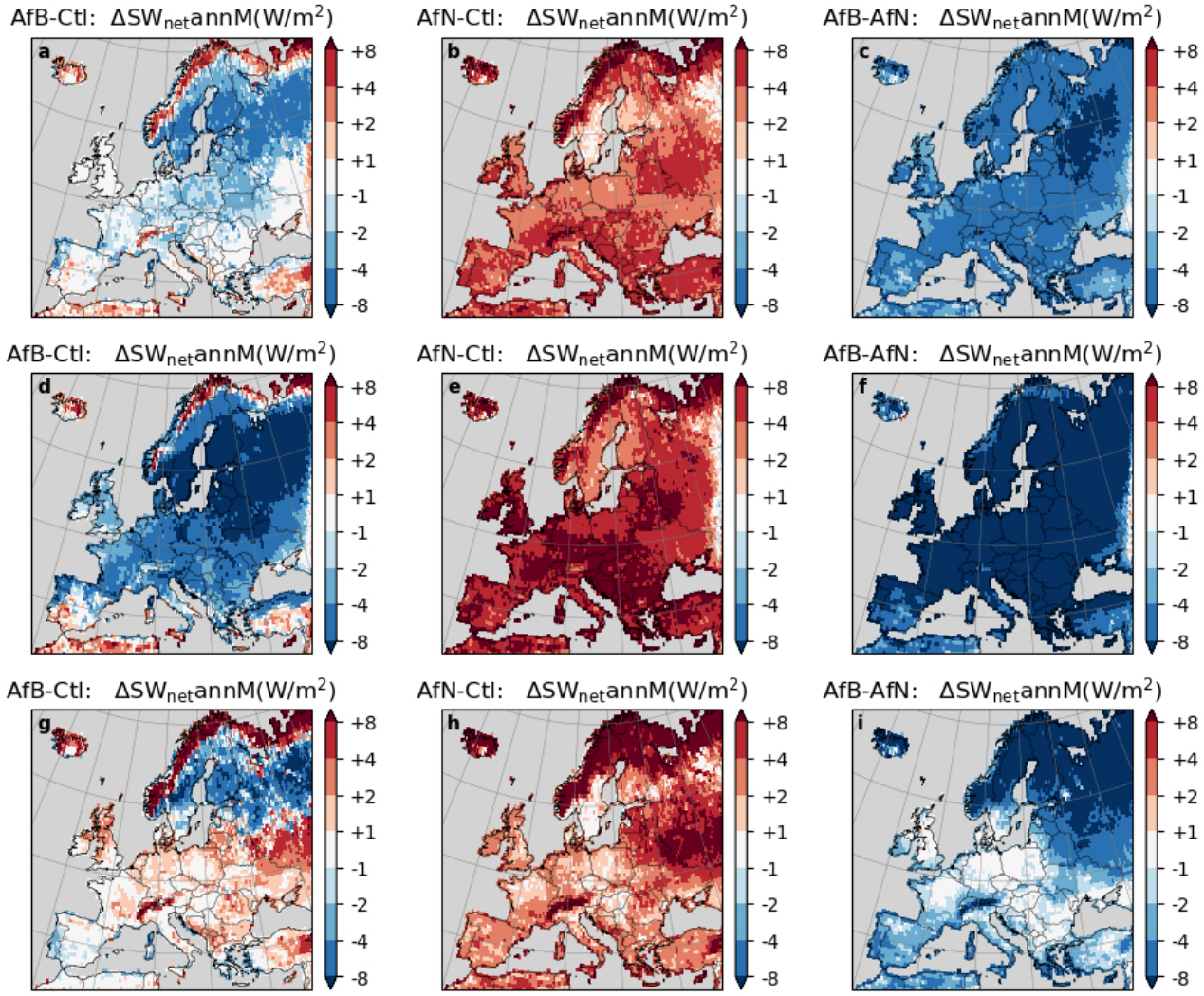

Supplementary Figure S27 | **a,d,g** Difference in $SWnet_{annM}$ (**a**), $SWnet_{sumM}$ (**d**) and $SWnet_{sprM}$ **g** between simulations with the forestation plus broadleaf scenario (AfB) and Ctl (AfB minus Ctl). **b,e,h** Difference in $SWnet_{annM}$ (**b**), $SWnet_{sumM}$ (**e**) and $SWnet_{sprM}$ **h** between simulations with the forestation plus conifer scenario (AfN) and Ctl (AfN minus Ctl). **c,f,i** Difference in $SWnet_{annM}$ (**c**), $SWnet_{sumM}$ (**f**) and $SWnet_{sprM}$ **i** between AfB and AfN (AfB minus AfN).

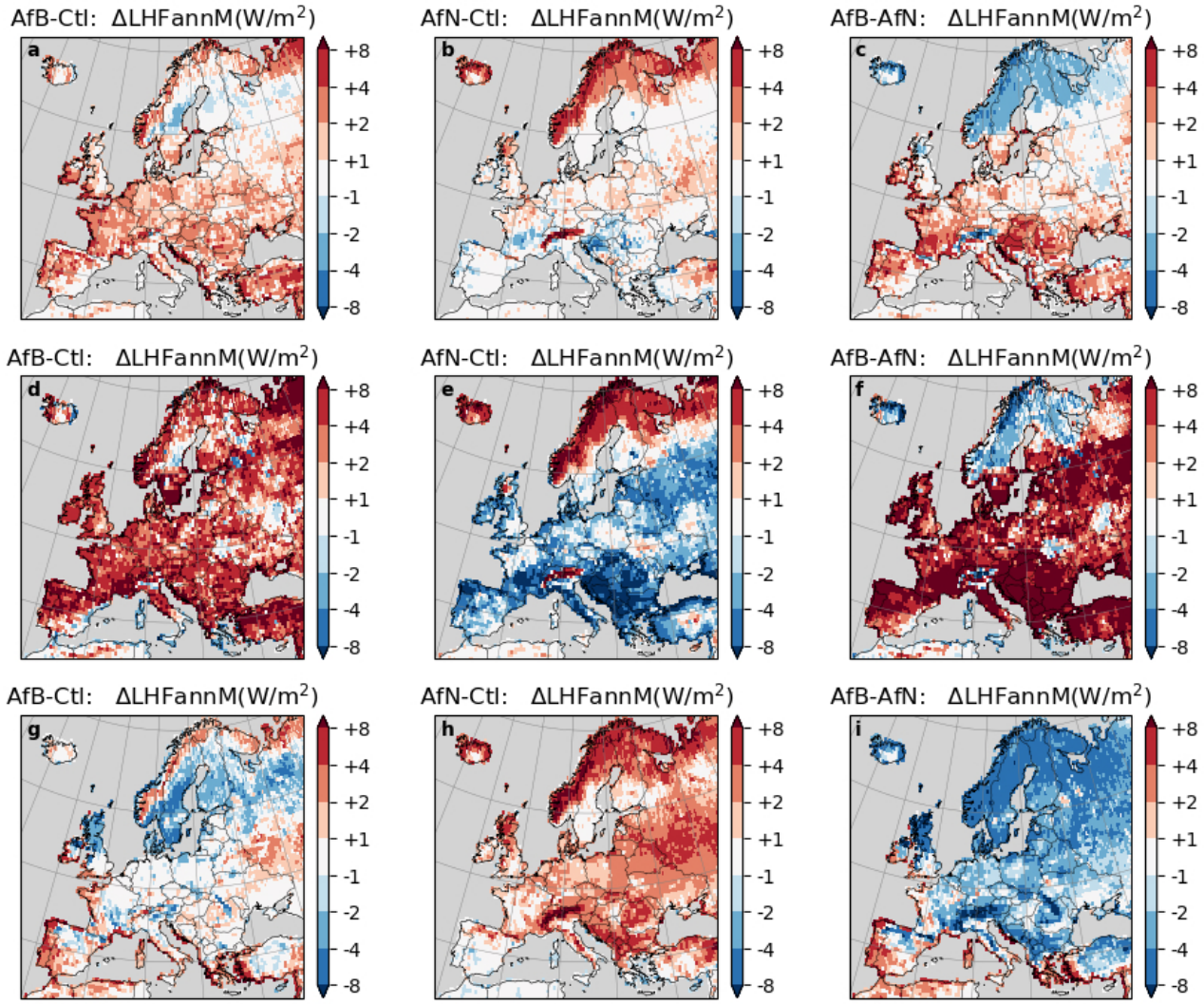

Supplementary Figure S28 | Same as Figure S27 but for Latent Heat Flux (LHF).

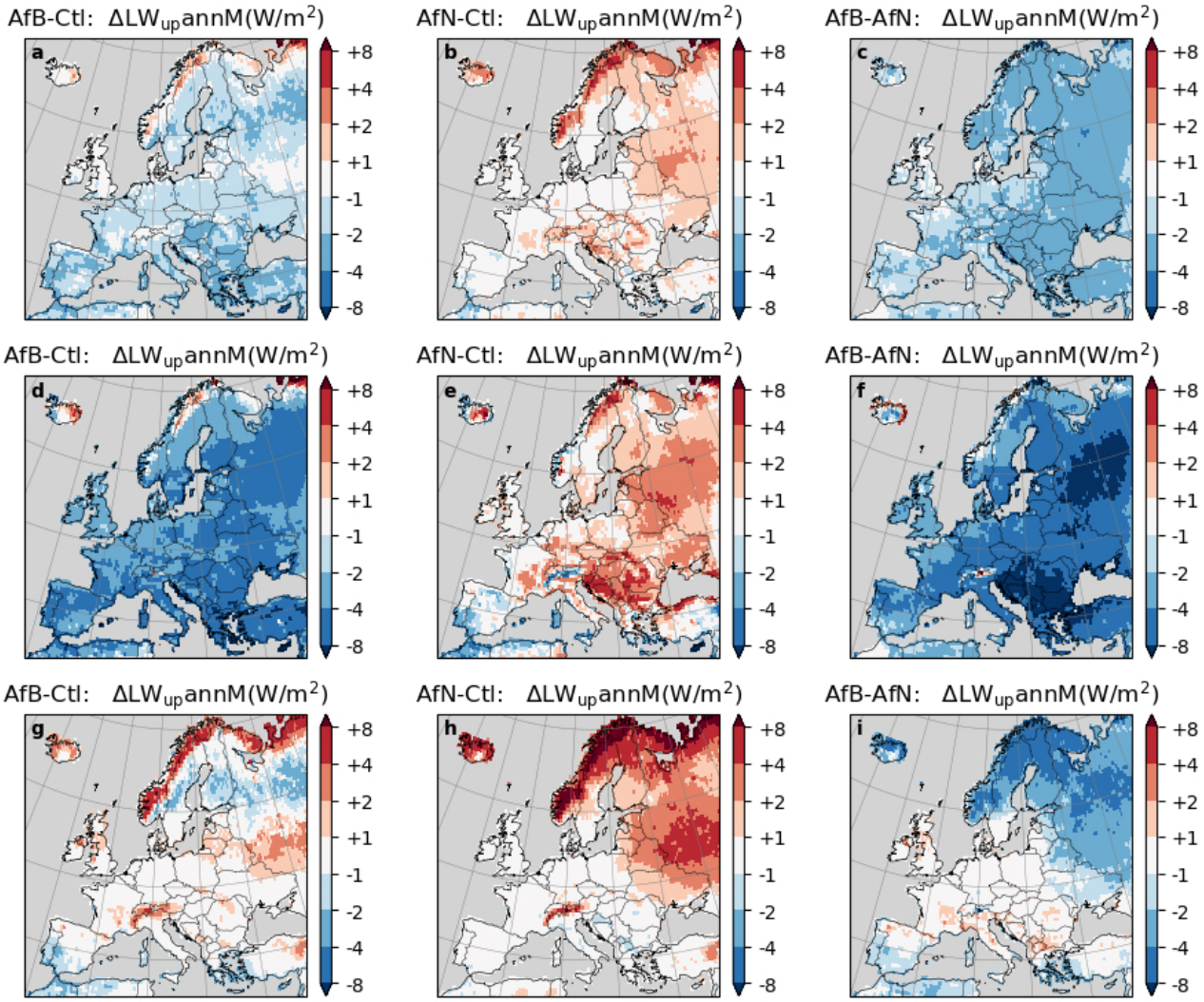

Supplementary Figure S29 | Same as Figure S27 but for upwelling longwave radiation (LWup).

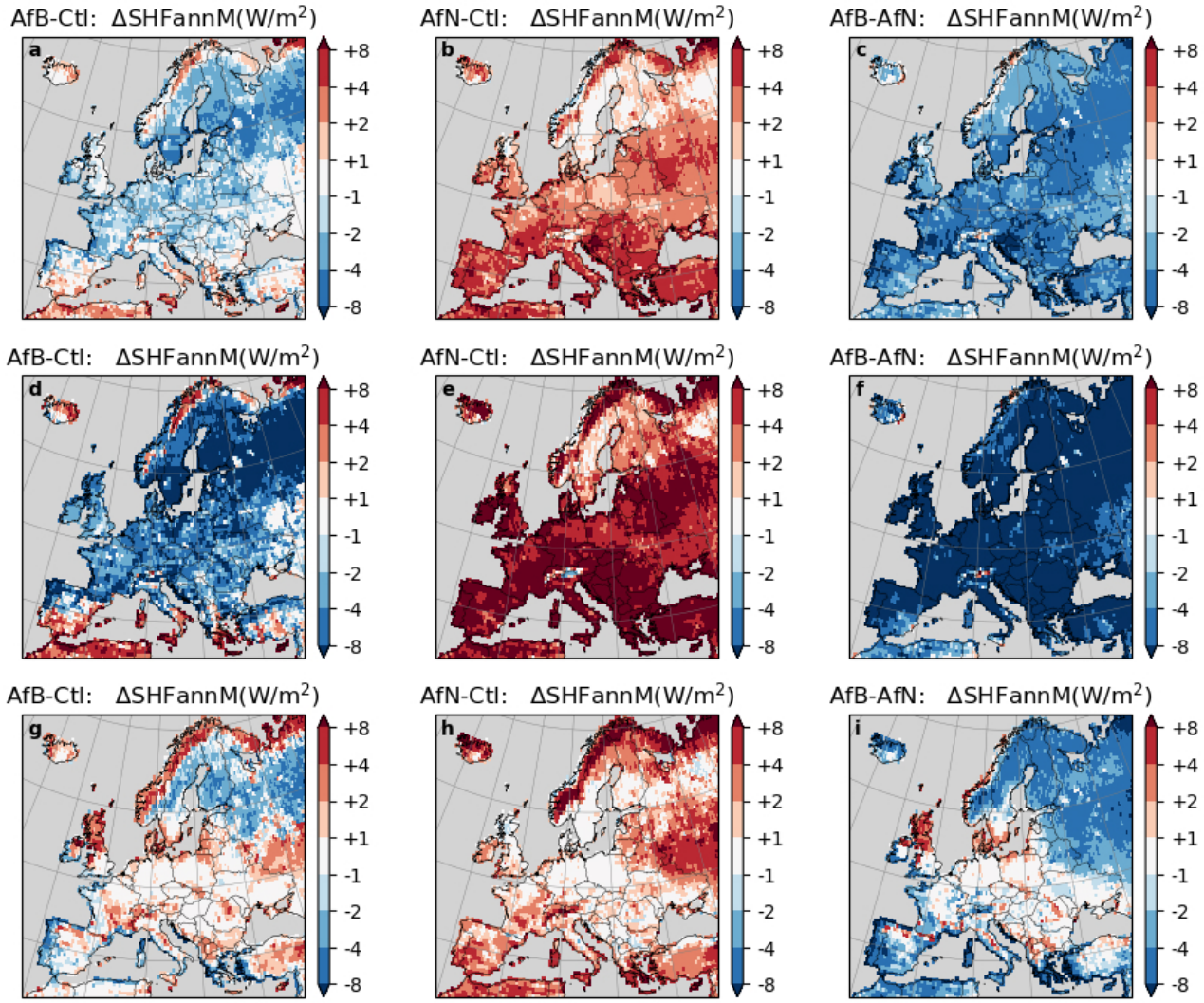

Supplementary Figure S30 | Same as Figure S27 but for Sensible Heat Flux (SHF).

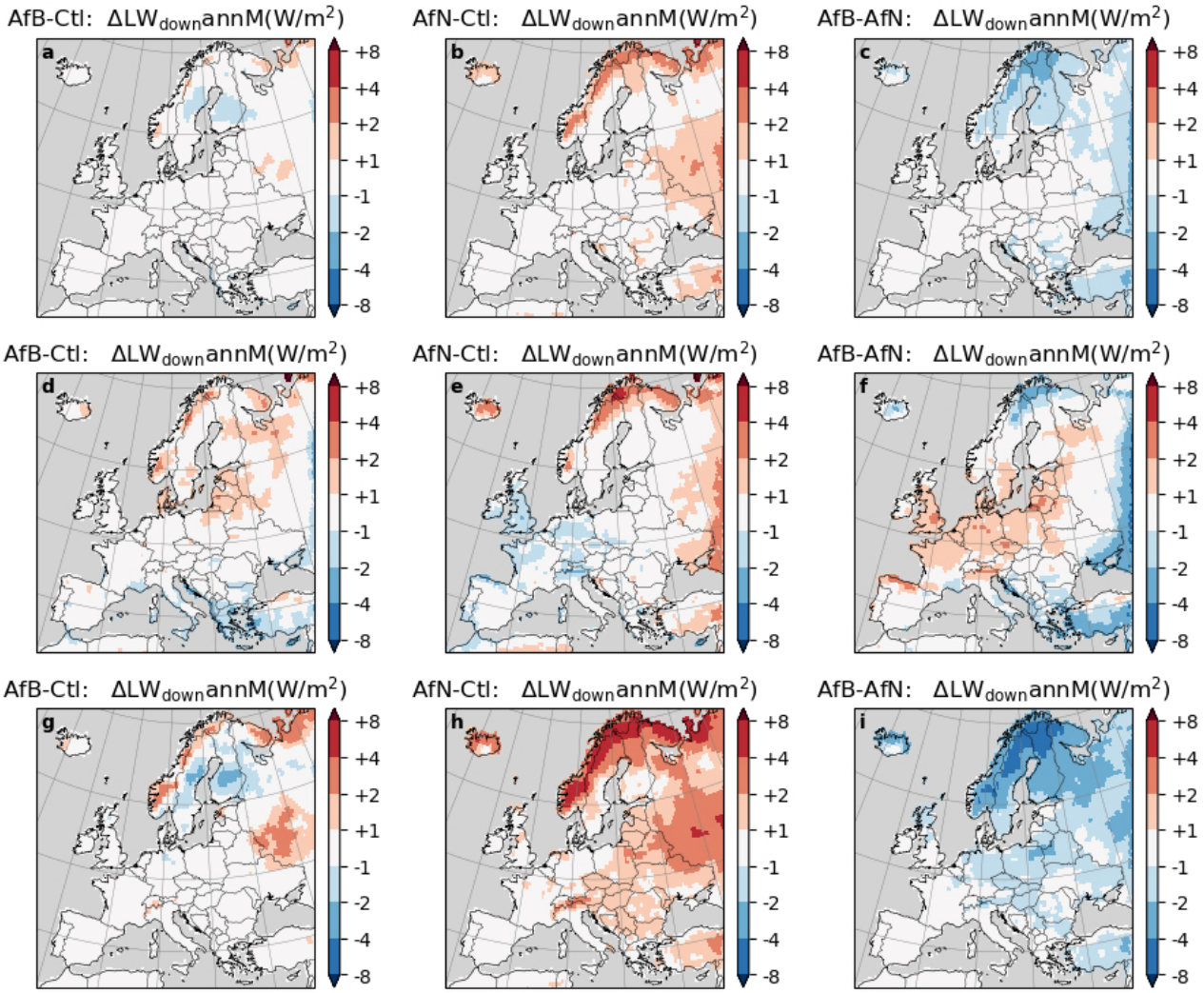

Supplementary Figure S31 | Same as Figure S27 but for downwelling longwave radiation (LWdown).

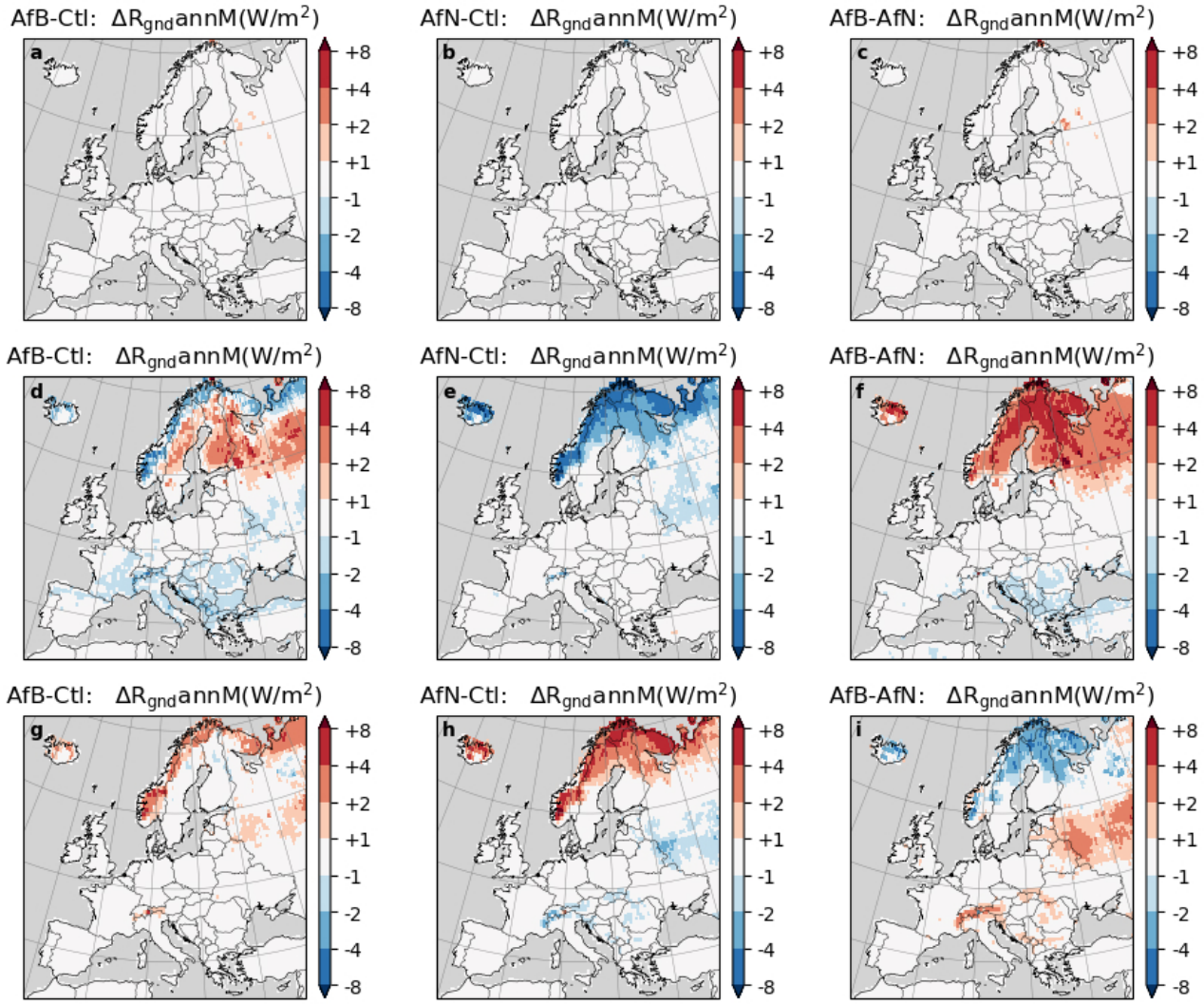

Supplementary Figure S32 | Same as Figure S27 but for ground heat flux (Rgnd).

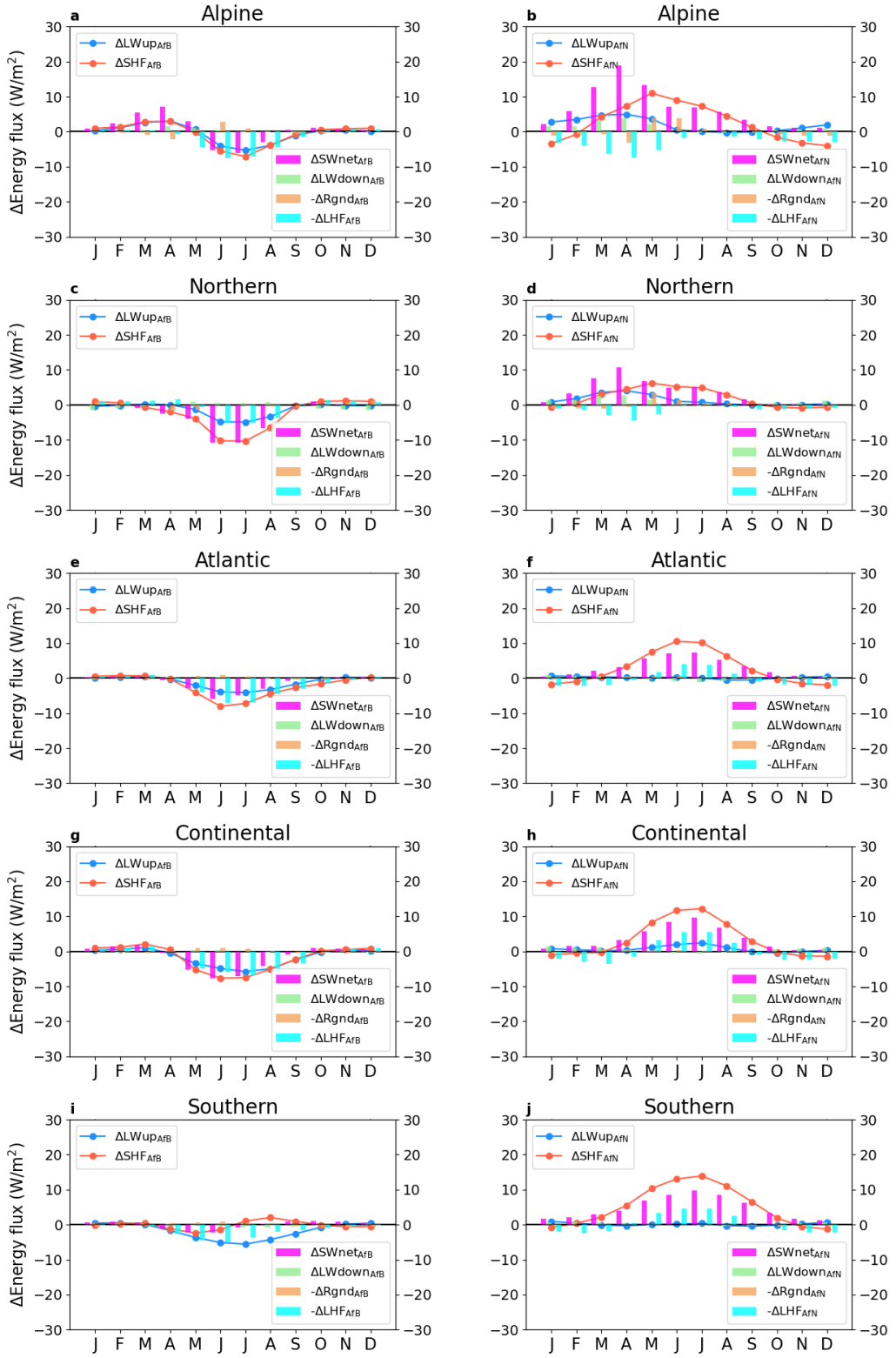

Supplementary Figure S33 | Changes in multi-year average monthly mean upwelling longwave radiation (LWup), sensible heat flux (SHF), and the contribution of other components, including net shortwave radiation (SWnet), downwelling longwave radiation (LWdown), ground heat flux (Rgnd), and latent heat flux (LHF), induced by forestation plus broadleaf (AfB) and forestation plus conifer (AfN) scenarios.

Impacts of AfB and AfN on T_{annX}, T_{sumX}, and T_{sprX} are similar to those on corresponding daily mean temperatures but with larger magnitudes (Figure S34). Regarding T_{annN}, T_{sumN}, and T_{sprN}, the main difference is that AfN also has cooling impacts over low-latitude regions, even exceeding the cooling of AfB in spring (Figure S35). This is possibly because of the enhanced canopy evaporation caused by higher LAI, which can be confirmed by the results of T_{monX} and T_{monN}. Changes in T_{monX} has a very similar temporal pattern to T_{monM} (Figure S14, S36). Interestingly, AfN has stable cooling impacts on T_{monN}, while AfB only has cooling impacts during summer over most regions, with various magnitudes and peaks in summer (Figure S37). This difference might be related to the different phenology types of conifer and broadleaf trees.

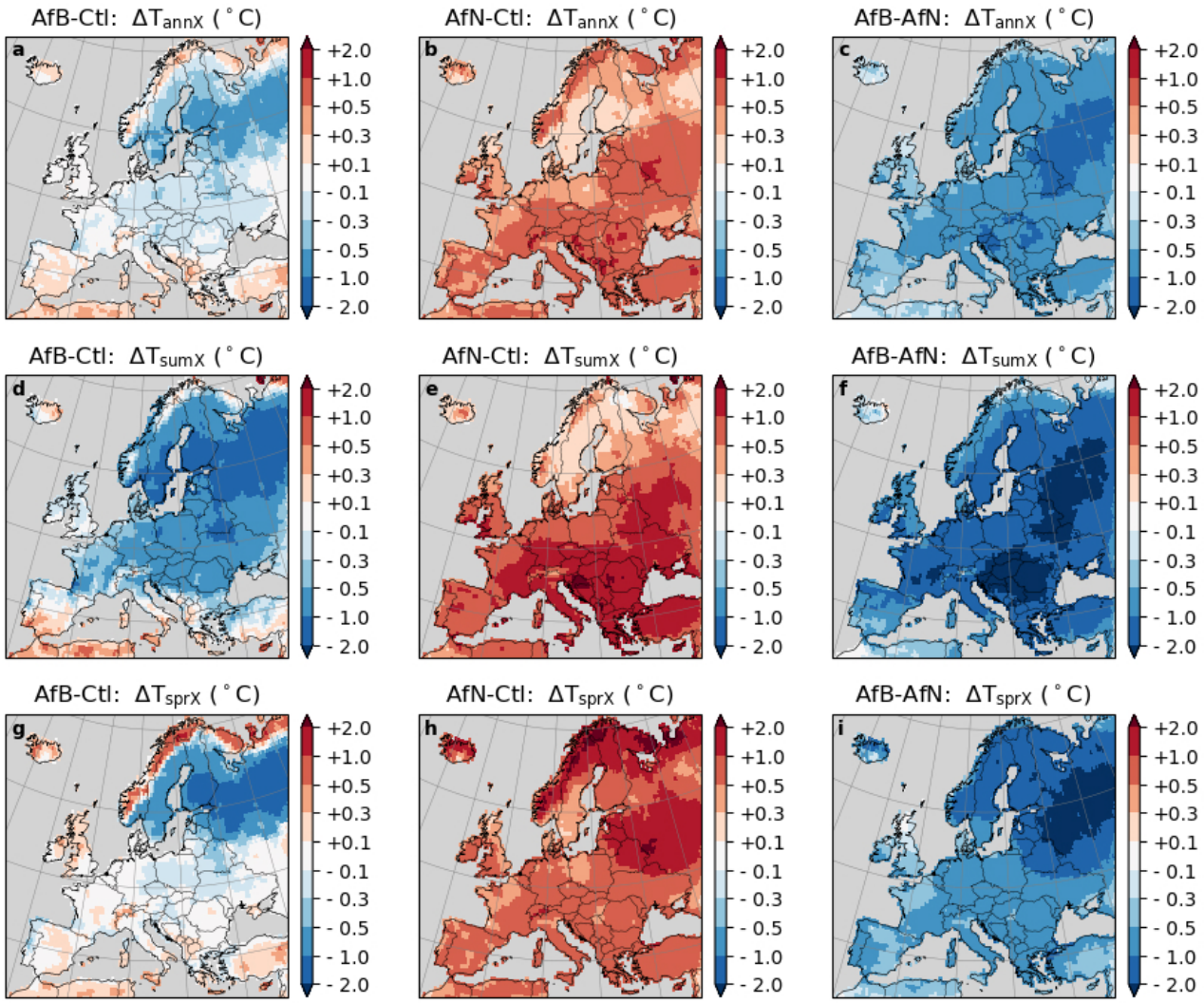

Supplementary Figure S34 | Same as Figure S26 but for multi-year average monthly mean daily maximum (T_{monX}).

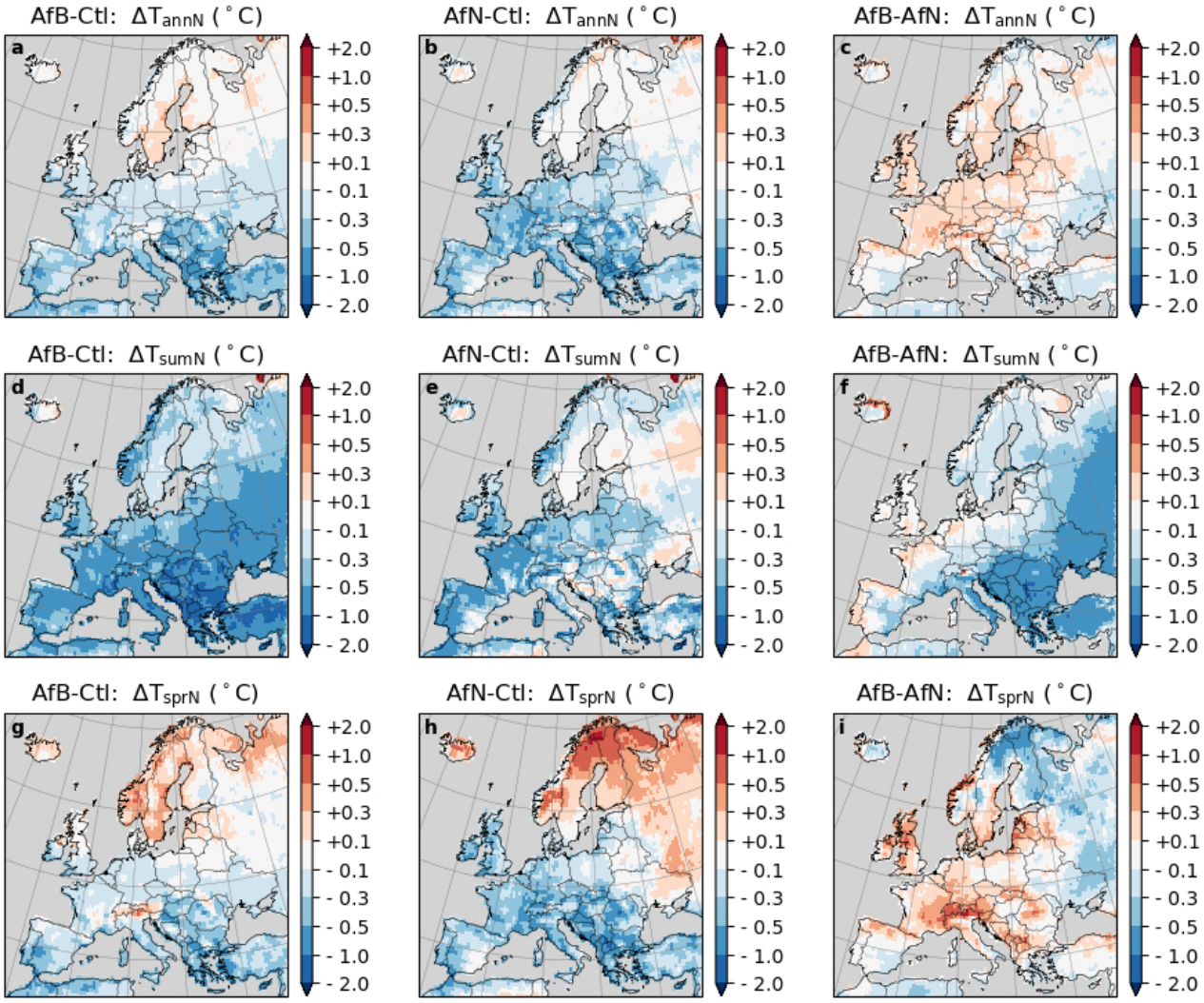

Supplementary Figure S35 | Same as Figure S26 but for multi-year average monthly mean daily minimum (T_{monN}).

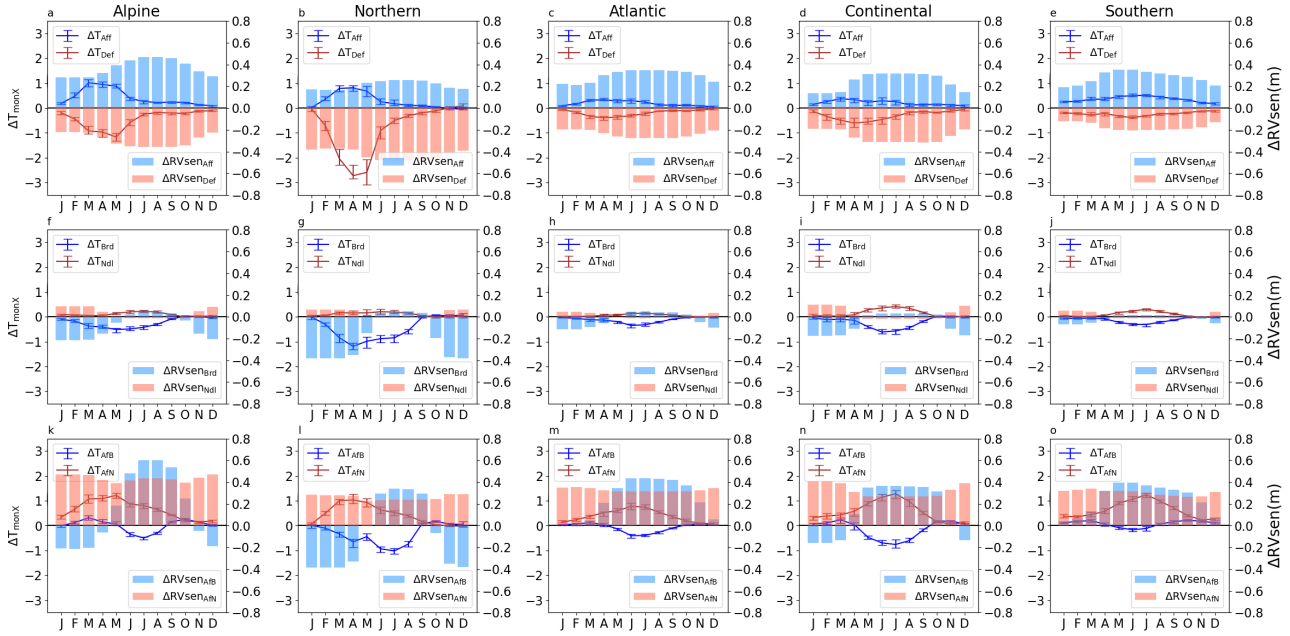

Supplementary Figure S36 | Same as Figure S14 but for multi-year average monthly mean daily maximum (T_{monX}).

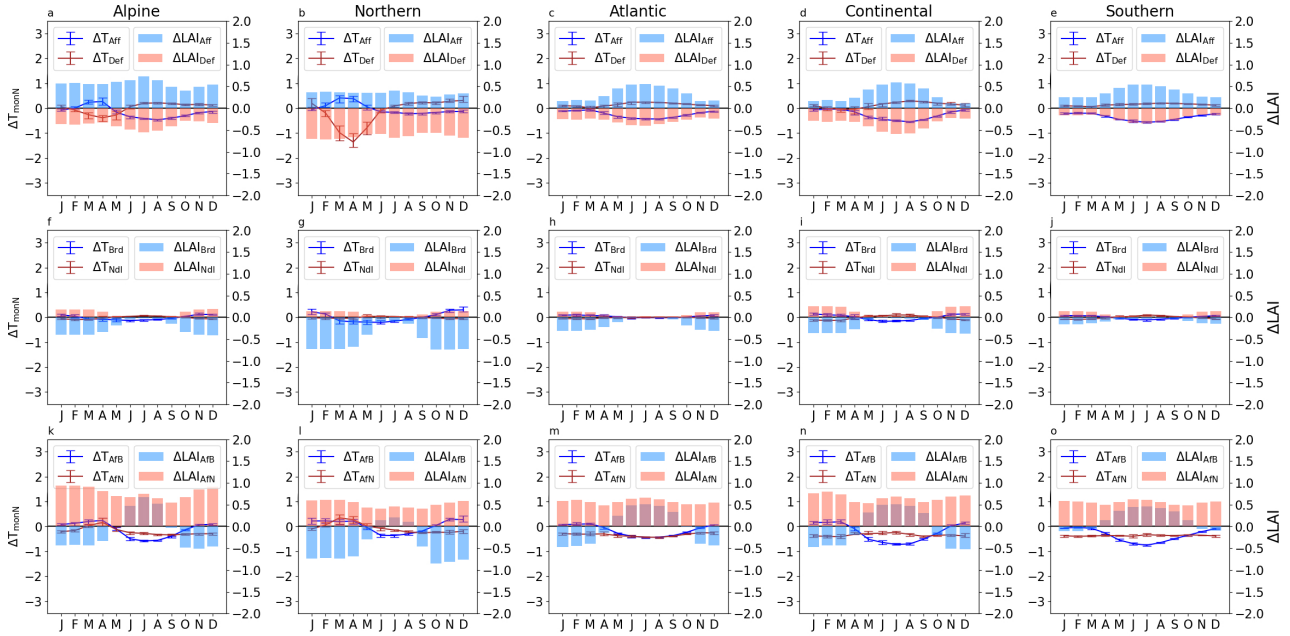

Supplementary Figure S37 | Same as Figure S14 but for multi-year average monthly mean daily maximum (T_{monN}).

2.4 Supplementary Note 4: Evaluation of COSMO – CLM^2 performance

Satellite-based land surface temperature (LST) datasets are commonly employed to examine the impacts of land use change. A previous study[4] utilized the Global Land Surface Satellite (GLASS) LST product, spanning 2002-2012, to compare adjacent forest land units with open land (grassland and cropland). In the present study, we focus on temperature data from forest and grassland land use tiles and compare the simulated LST differences between these land types within the same grid cells. The results (Figure S38) indicate that the model successfully reproduces the spatial pattern of the annual mean daily maximum LST difference, but fails to simulate the significant difference observed in the annual mean daily minimum LST. Another study[5], based on the Moderate Resolution Imaging Spectroradiometer (MODIS) LST product (2008-2012), employed a moving-window algorithm to establish a linear relationship between forest cover and LST feedback, and quantified the maximum potential impact of forest cover change or tree species transition. In this study, we compare the differences between the simulations Def and Aff, representing deforestation (forest replaced by grassland and cropland, Figure S39), and between Afforestation plus transition to conifer trees (AfN) and AfB (Figure S40), representing forest type transition (from deciduous broadleaf to evergreen conifer forests). Comparison shows that both results agree on the warming effect of deforestation on summer maximum LST and the cooling effect on spring minimum LST. Regarding tree species transition, although there is a limited number of valid grid cells in the observation-based dataset, the majority of grid cells show a warming effect on maximum LST in summer when transitioning from broadleaf to conifer forests, which shares the signal with simulations.

In addition to directly comparing LST, an alternative approach to assessing the impacts of land use and land management change involves utilizing a surface energy balance algorithm, which leverages multiple satellite observations of land properties and energy fluxes[6]. This method enables the calculation of the radiative impacts of forest changes. By comparing the LST differences between conifer forests, broadleaf forests, and grassland in the Ctl simulation, we can assess the agreement with the dataset from[6]. The results (Figure S41 and S42) indicate that the model successfully replicates the cooling effects of afforestation (both conifer and broadleaf) in low-latitude regions during the summer, and the warming effect associated with the transition from broadleaf to conifer forests is also well captured. Given that LST is highly correlated with surface air temperature[3], we are confident in the signal of the BGP impacts simulated by COSMO-CLM^2, particularly for the mean daily mean and maximum temperatures of the summer.

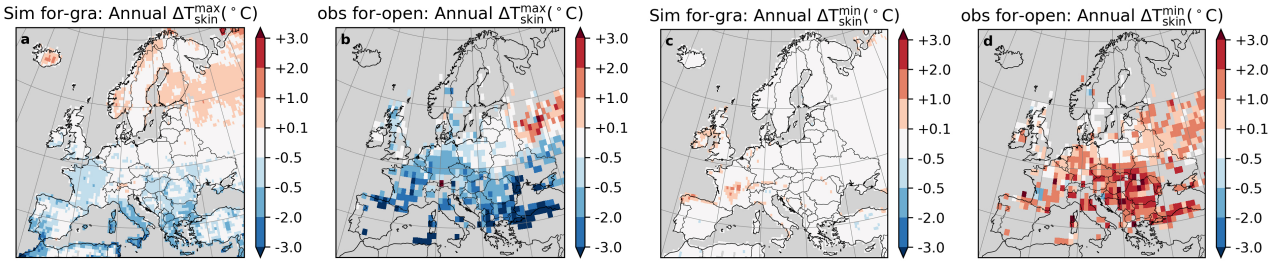

Supplementary Figure S38 | **a,c** Simulated difference in multi-year (2025-2059) mean daily maximum (T^{max}_{skin}) and daily minimum land surface temperature (T^{min}_{skin}) between the forest and grassland land-use tile in the control simulation. **b,d** Observation-based difference in multi-year (2002-2012) mean T^{max}_{skin} and T^{min}_{skin} [4].

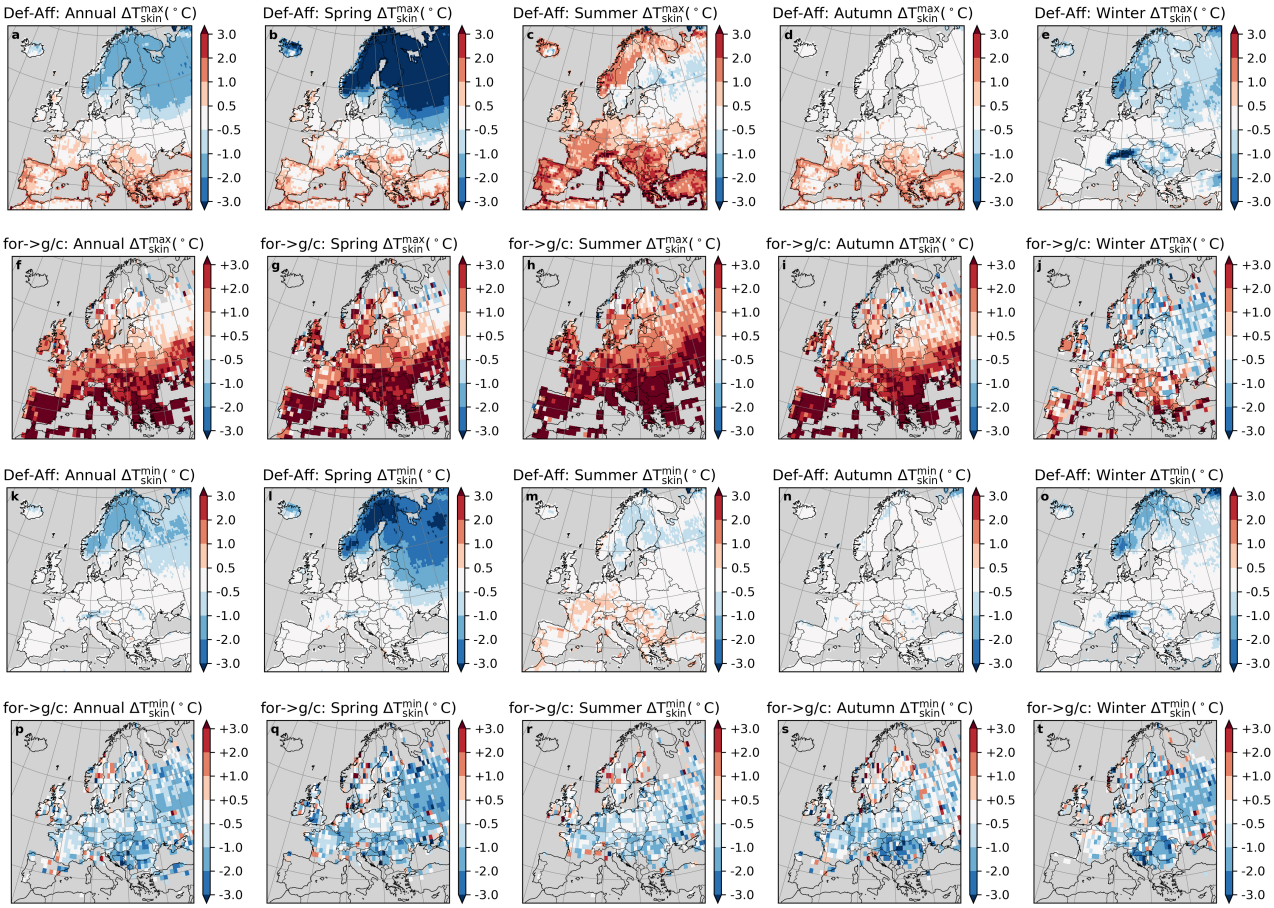

Supplementary Figure S39 | **a-e, k-o** Simulated difference in multi-year (2025-2059) mean daily maximum (T^{max}_{skin}) and daily minimum land surface temperature (T^{min}_{skin}) between the forestation and deforestation scenarios (Def-Aff). **b-f,p-t** Observation-based potential of changes in multi-year (2008-2012) mean T^{max}_{skin} and T^{min}_{skin} because of deforestation [5].

2.5 Supplementary Note 5: Results from additional sensitivity tests

Compared to land-use change, modifying canopy height or LAI index alone has less impact on temperature (Figure S43). Increasing canopy height slightly increases T_{sumM}, which could be due to the increased roughness, while increased LAI provides more evaporative cooling impacts in summer. Interestingly, Decreasing LAI in spring shows cooling effects in high-latitude areas,

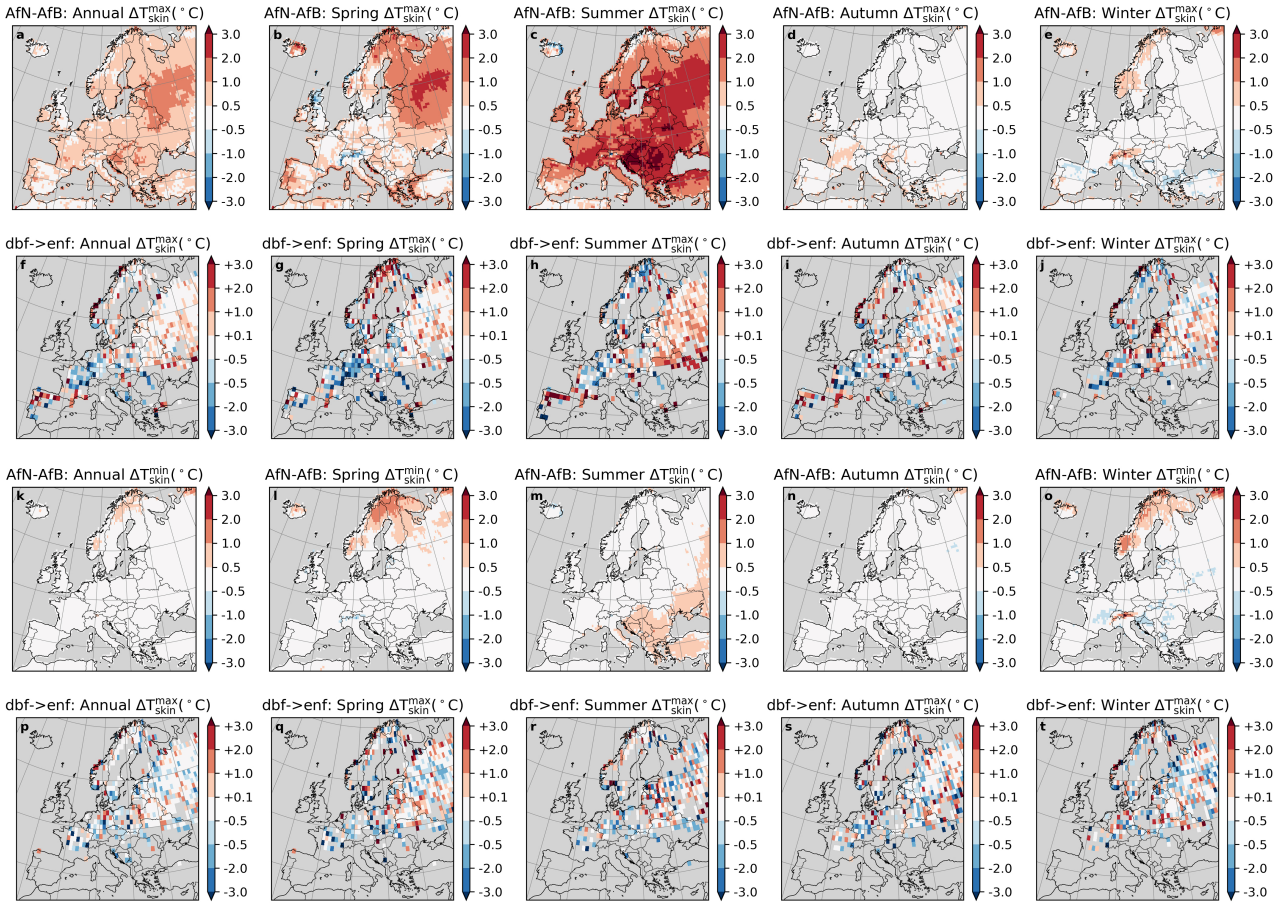

Supplementary Figure S40 | **a-e, k-o** Simulated difference in multi-year (2025-2059) mean daily maximum (T^{max}_{skin}) and daily minimum land surface temperature (T^{min}_{skin}) between the combining scenario of forestation and transition from broadleaf to conifer forests and the opposite transition (AfN-AfB). **b-f,p-t** Observation-based potential of changes in multi-year (2008-2012) mean T^{max}_{skin} and T^{min}_{skin} because of the transition from broadleaf to conifer forests[5].

which could be due to albedo changes. However, in this study, the forest health scenarios are relatively conservative (multiplied by 1.5 or divided by 1.5), and more extreme scenarios may have more pronounced impacts. Please note that these scenarios are highly idealised and may not reflect the possible changes in reality.

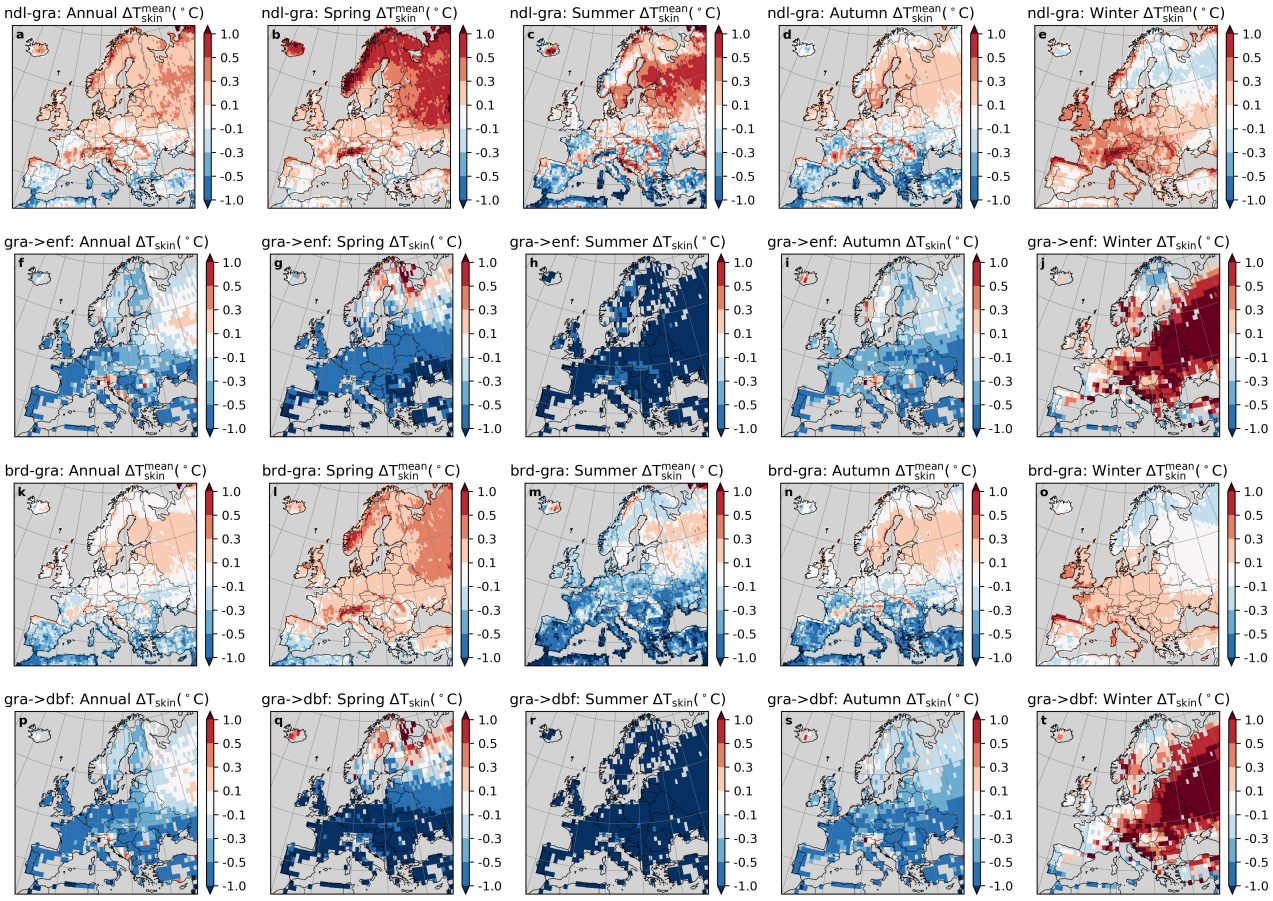

Supplementary Figure S41 | **a-e, k-o** Simulated difference in multi-year (2025-2059) mean daily maximum (T_{skin}^{max}) and daily minimum land surface temperature (T_{skin}^{min}) between the conifer forest and grassland land-use tiles, and between the broadleaf forest and grassland land-use tiles. **b-f,p-t** Calculated radiative impacts of the land-use change from grassland to conifer or broadleaf forest[6].

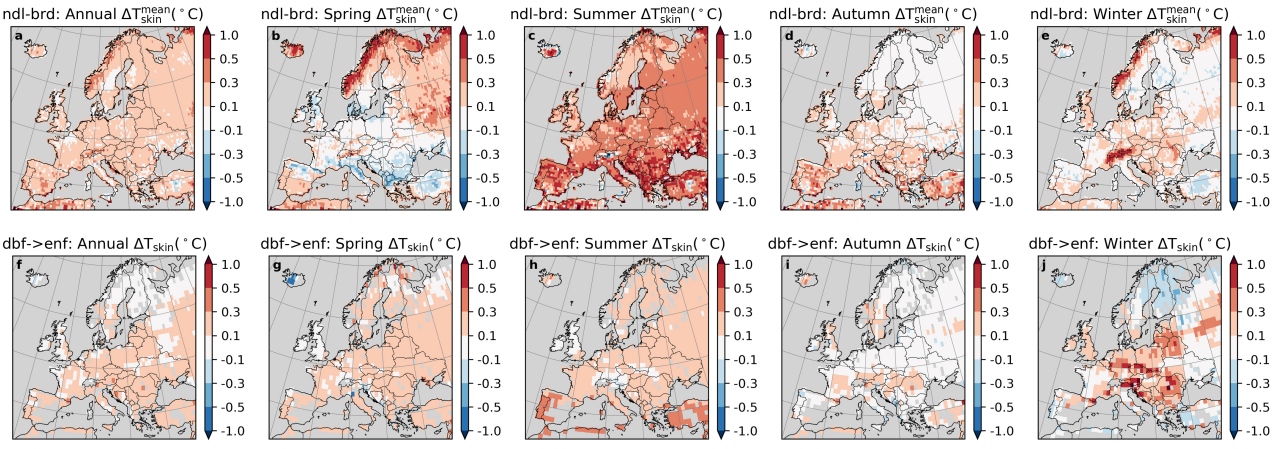

Supplementary Figure S42 | **a-e** Simulated difference in multi-year (2025-2059) mean daily maximum (T_{skin}^{max}) and daily minimum land surface temperature (T_{skin}^{min}) between the broadleaf and conifer land-use tiles. **b-f** Calculated radiative impacts of the land-use change from broadleaf to conifer forest[6].

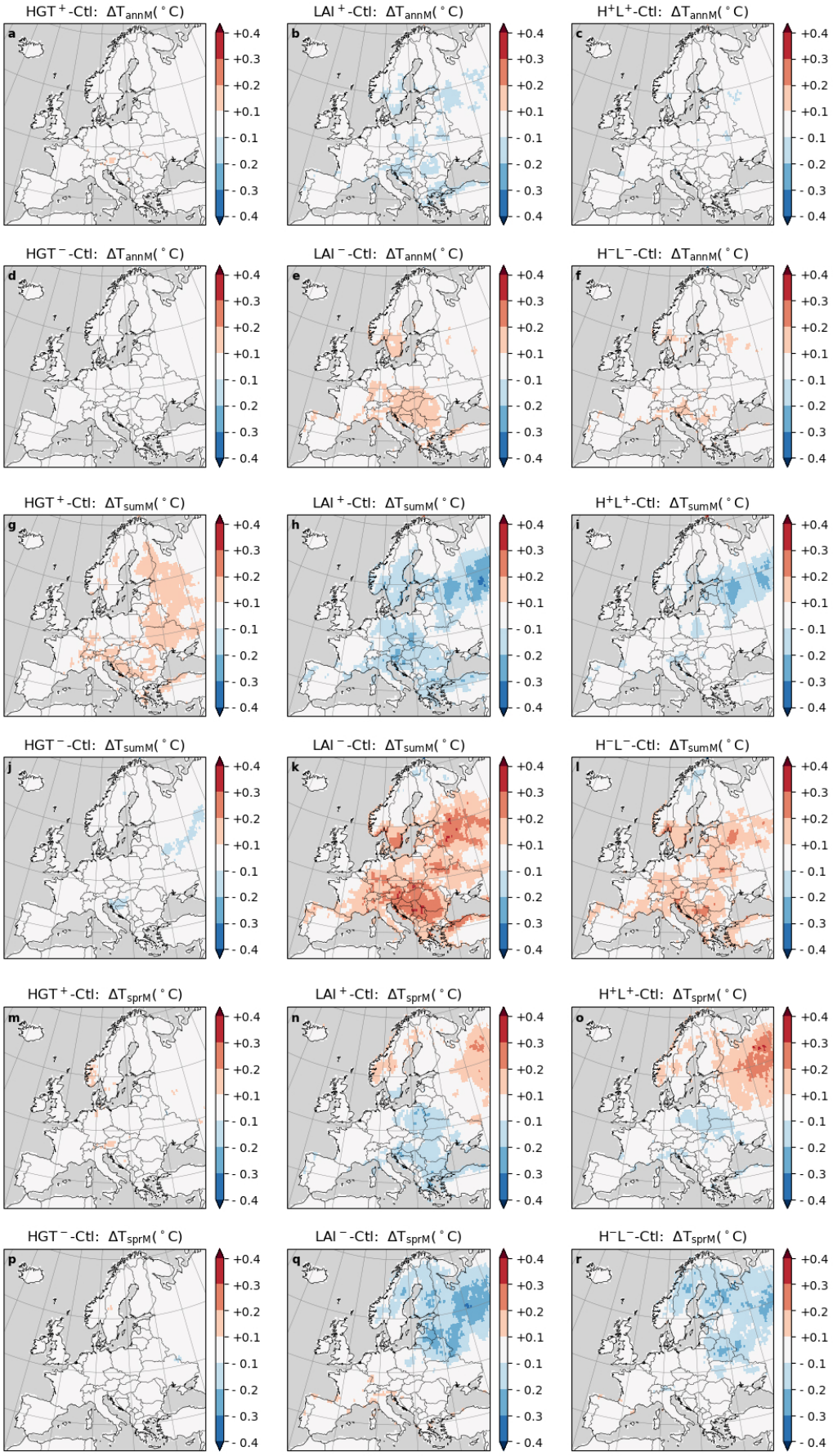

Supplementary Figure S43 | Same as Figure S7 but for sensitivity test (HGT^+: Canopy heights multiplied by 1.5; HGT^-: Canopy heights divided by 1.5; LAI^+: LAI multiplied by 1.5; LAI^-: LAI divided by 1.5; H^+L^+: both canopy heights and LAI multiplied by 1.5; H^-L^-: both canopy heights and LAI divided by 1.5) scenarios.

Supplementary References

[1] Yan, H., Wang, S., Billesbach, D., Oechel, W., Zhang, J., Meyers, T., Martin, T., Matamala, R., Baldocchi, D., Bohrer, G. & Others Global estimation of evapotranspiration using a leaf area index-based surface energy and water balance model. *Remote Sensing Of Environment*. **124** pp. 581-595 (2012)

[2] Flanner, M., Shell, K., Barlage, M., Perovich, D. & Tschudi, M. Radiative forcing and albedo feedback from the Northern Hemisphere cryosphere between 1979 and 2008. *Nature Geoscience*. **4**, 151-155 (2011)

[3] Good, E., Ghent, D., Bulgin, C. & Remedios, J. A spatiotemporal analysis of the relationship between near-surface air temperature and satellite land surface temperatures using 17 years of data from the ATSR series. *Journal Of Geophysical Research: Atmospheres*. **122**, 9185-9210 (2017)

[4] Li, Y., Zhao, M., Motesharrei, S., Mu, Q., Kalnay, E. & Li, S. Local cooling and warming effects of forests based on satellite observations. *Nature Communications*. **6**, 6603 (2015)

[5] Duveiller, G., Hooker, J. & Cescatti, A. The mark of vegetation change on Earth's surface energy balance. *Nature Communications*. **9**, 679 (2018)

[6] Bright, R., Davin, E., O'Halloran, T., Pongratz, J., Zhao, K. & Cescatti, A. Local temperature response to land cover and management change driven by non-radiative processes. *Nature Climate Change*. **7**, 296-302 (2017)